

EcoDes-DK15: High-resolution ecological descriptors of vegetation and terrain derived from Denmark's national airborne laser scanning data set

Jakob J. Assmann¹, Jesper E. Moeslund², Urs A. Treier^{1,3}, Signe Normand^{1,3}

¹Department of Biology - Ecoinformatics and Biodiversity, Aarhus University, Aarhus, 8000, Denmark

²Department of Ecoscience - Biodiversity, Aarhus University, Rønde, 8410, Denmark

³Department of Biology - Center for Sustainable Landscapes Under Global Change, Aarhus University, Aarhus, 8000, Denmark

Correspondence to: Jakob J. Assmann (j.assmann@bio.au.dk)

Abstract

Biodiversity studies could strongly benefit from three-dimensional data on ecosystem structure derived from contemporary remote sensing technologies, such as Light Detection and Ranging (LiDAR). Despite the increasing availability of such data at regional and national scales, the average ecologist has been limited in accessing them due to high requirements on computing power and remote sensing knowledge. We processed Denmark's publicly available national Airborne Laser Scanning (ALS) data set acquired in 2014/15 together with the accompanying elevation model to compute 70 rasterized descriptors of interest for ecological studies. With a grain size of 10 m, these data products provide a snapshot of high-resolution measures including vegetation height, structure and density, as well as topographic descriptors including elevation, aspect, slope and wetness across more than forty thousand square kilometres covering almost all of Denmark's terrestrial surface. The resulting data set is comparatively small (~94 GB, compressed 16.8 GB) and the raster data can be readily integrated into analytical workflows in software familiar to many ecologists (GIS software, R, Python). Source code and documentation for the processing workflow are openly available via a code repository, allowing for transfer to other ALS data sets, as well as modification or re-calculation of future instances of Denmark's national ALS data set. We hope that our high-resolution ecological vegetation and terrain descriptors (EcoDes-DK15) will serve as an inspiration for the publication of further such data sets covering other countries and regions and that our rasterized data set will provide a baseline of the ecosystem structure for current and future studies of biodiversity, within Denmark and beyond. The full data set is available on Zenodo: <https://doi.org/10.5281/zenodo.4756556> and a 5 MB teaser subset can be found on the GitHub code repository: https://github.com/jakobjassmann/ecodes-dk-lidar/blob/master/manuscript/figure_7/EcoDes-DK15_teaser.zip.

30 **1 Introduction**

31 Over the last decades, airborne laser scanning (ALS) has become an established data source for providing fine-resolution
32 measures of terrain and vegetation structure in ecological research (Moeslund et al., 2019; Guo et al., 2017; Zellweger et al.,
33 2016). Despite its informative potential and the increasing number of openly available ALS data sets with regional and national
34 extents (Vo et al., 2016), the uptake of these data sets for large-scale ecological research and applications (such as monitoring
35 and conservation) has remained comparatively low (Bakx et al., 2019). The low uptake is likely a consequence of the
36 considerable challenges that remain in handling these very large data sets, which require specialist expertise and software, as
37 well as substantial amounts of data storage and processing power (Meijer et al., 2020; Vo et al., 2016; Pfeifer et al., 2014).
38 Here, we address this issue for Denmark by providing a compact set of ecologically relevant measures of terrain characteristics
39 and vegetation structure derived as raster outputs from the country's national ALS data set with a grain size of 10 m x 10 m.

40 The typical output from an ALS survey is a so-called point cloud that describes the physical structure of the surveyed area in
41 three-dimensional space (Bakx et al., 2019; Vierling et al., 2008). In brief, short laser pulses are sent out from a Light Detection
42 and Ranging (LiDAR) sensor mounted on an airplane (or drone) and reflected by surfaces such as bare ground, plants or
43 buildings. The return timing of the reflected signal is measured and - with the help of information on the sensor's orientation
44 and position - the precise location of the reflecting surface is determined in geographic space (Vierling et al., 2008). If an
45 object intercepting the light pulse is smaller than the beam's footprint (e.g., a leaf or a branch of a tree), some of the light may
46 travel on and trigger a reflection from a second surface (e.g., understory vegetation or the forest floor). A single light pulse
47 might therefore generate two or even more returns, allowing - to some degree - for the penetration of forest canopies
48 (Ackermann, 1999). Often, the raw signal is processed by the survey provider and the resulting data is delivered to the end
49 user in the form of a point cloud of discrete returns, where each point is associated with information on geographic location,
50 return strength (amplitude), return number, acquisition timing etc. (Vo et al., 2016). For ALS data sets with large extents -
51 such as Denmark's nationwide data set "DHM/Punktsky" - outputs from many survey flights are co-registered and merged,
52 resulting in very large point clouds with hundreds of billions of points and data volumes of multiple Terabytes
53 (Geodatastyrelsen, 2015). For further information on ALS data acquisition, we recommend Vo et al. (2016), Vierling et al.
54 (2008) and Wagner et al. (2006).

55 Based on point position and neighbourhood context it is possible to separate ground and vegetation returns in ALS point
56 clouds, allowing for the calculation of descriptors of terrain and vegetation structure. Filtering bare ground from the point
57 cloud may be achieved with algorithms (Moudrý et al., 2020; Sithole and Vosselman, 2004), while more complex segmentation
58 of the point clouds into object classes (such as vegetation, buildings, etc.) is done manually or with the help of supervised
59 machine learning (see Lin et al., 2020 for a recent overview). Early applications for ALS were focussed on generating simple
60 digital elevation models (DEMs), city and landscape planning, as well as forestry (Ackermann, 1999), but over the last decades
61 applications have expanded into other fields, including amongst others the calculation of terrain and vegetation measures for

62 ecological research. Terrain derived measures of ecological interest include topographic slope, aspect (i.e., slope direction),
63 solar irradiation, wetness etc. (e.g., Moeslund et al., 2019; Zellweger et al., 2016; Ceballos et al., 2015), and vegetation
64 structural descriptors include vegetation density, canopy height diversity, canopy roughness and many more (e.g., Bakx et al.,
65 2019; Moeslund et al., 2019; Coops et al., 2016). It is important to note that point cloud characteristics may limit the type of
66 measures that can be meaningfully derived from ALS data (Bakx et al., 2019). This applies especially to the point cloud
67 density, which needs to be high enough to meaningfully resolve the structure of understory layers in forests (Bakx et al., 2019)
68 or ecosystems with vegetation of low stature such as grasslands or tundra (Boelman et al., 2016). Nonetheless, even simpler
69 ALS derived descriptors of terrain and vegetation structure can be of high value for ecological applications, as fieldwork-
70 derived alternatives are often too costly and difficult to collect over large extents (Vierling et al., 2008).

71 ALS data has provided critical information for research on biodiversity and habitat characteristics over the recent years, and
72 its importance in ecological research is likely to increase in the future. Numerous biodiversity studies have successfully
73 deployed ALS to study organisms like plants (Mao et al., 2018; Lopatin et al., 2016; Zellweger et al., 2016; Ceballos et al.,
74 2015; Moeslund et al., 2013; Leutner et al., 2012), fungi (Peura et al., 2016; Thers et al., 2017), bryophytes, lichens (Moeslund
75 et al., 2019), mammals (Tweedy et al., 2019; Froidevaux et al., 2016) and birds (see Bakx et al. (2019) for a comprehensive
76 review) both in open landscapes and in forests. These studies have all emphasized the value of ALS for representing fine-scale
77 (~ 10 m resolution) terrain or vegetation structural variation important to local biodiversity patterns. Furthermore, Valbuena
78 et al. (2020) recently considered ALS data to be one of the key resources for deriving ecosystem morphological traits in the
79 global assessment of Essential Biodiversity Variables (EBVs). Finding ways of making regional and nationwide ALS data
80 more accessible to the average ecologist is therefore not only a critical priority for accelerating research on regional biodiversity
81 patterns and species - habitat relationships, but also for the facilitation of global assessments such as those carried out by
82 IPBES (2019) and alike.

83 To open up opportunities for researchers and practitioners not familiar with ALS processing or without access to the required
84 facilities, we present a new national ALS based data set for Denmark primarily aimed at ecological research with possible uses
85 in other disciplines. With a grain size of 10 m, these ecological descriptor (EcoDes) rasters provide a snapshot of high-
86 resolution measures of vegetation height, structure and density, as well as topographic descriptors including elevation, aspect,
87 slope and wetness for almost all of Denmark's terrestrial surface between spring 2014 and summer 2015 (DK15). In this
88 publication, we a) describe the source data and outline the processing workflow (Sect. 2.1-2.3), b) summarise the data set's
89 main characteristics (Sect. 3.1-3.2), c) describe each descriptor in detail and highlight its use and limitations (Sect. 3.3-3.4), d)
90 provide guidance on data access and illustrate how the data could be used in an example of ecological landscape classification
91 (Sect. 4). We finish by e) briefly discussing the general limitations of the data set and processing workflow, as well as providing
92 perspectives on how the presented data can be complemented with other data sources (Sect. 5). We hope that ease of access

93 and thorough documentation of the EcoDes-DK15 data set will encourage uptake and facilitate the development of future
94 versions of similar data sets in Denmark and beyond.

95 **2 Source data and processing workflow overview**

96 **2.1 Denmark - geography and ecology**

97 Located in Northern Europe, Denmark (without Greenland and the Faroe Islands) has an approximate land area of 43 thousand
98 square kilometres, comprising the large peninsula of Jutland and 443 named islands. The relatively flat (highest point is 171
99 m above sea level) landscape predominantly consists of arable land and production forest with relatively small patches of
100 natural or semi-natural areas such as heathlands, grasslands, fresh and salt meadows, bogs, dunes, lakes, streams and deciduous
101 forests.

102 **2.2 ALS and elevation source data**

103 The Danish elevation model (DHM) is an openly available nationwide data set providing various products based on ALS data.
104 Here, we used the DHM/Point-cloud (DHM/Punktsky), the classified georeferenced ALS point cloud product, and the
105 DHM/Terrain (DHM/Terræn), the digital elevation model product derived from the point cloud. The DHM data set is currently
106 maintained by the Agency for Data Supply and Efficiency, Denmark (<https://sdfe.dk/>) and, at the time of writing, can be
107 downloaded from <https://kortforsyningen.dk/> (continuously updated with new survey data) and <https://datafordeler.dk/>
108 (versioned). While almost all of Denmark's terrestrial surface was covered by ALS surveys in 2014/15, currently none of the
109 products provided by the agency contains data exclusively from these surveys. We therefore merged three different versions
110 of the source data to obtain a dataset that reflects the state of the vegetation in 2014/15 as best as possible, by only containing
111 vegetation data from 2014/15 and limited amounts from 2013 (Table 1, Sect. 3.6.3; see GitHub code repository for a detailed
112 description of the merger and more information on the source data sets). The DHM/Point-cloud product is a collection of 1 x
113 1 km tiles of three-dimensional point clouds with attributes such as position, intensity, point source ID, or classification. Point
114 classification follows the ASPRS LAS 1.3 standard (ASPRS, 2011), including for example ground, vegetation, and buildings.
115 The point density is on average 4-5 points per square meter with a horizontal and vertical accuracy of 0.15 and 0.05 metres,
116 respectively. Additional information on the data sets can be found in Geodatastyrelsen (Geodatastyrelsen, 2015 - in Danish),
117 Thers et al. (2017), Nord-Larsen et al (2017) and in the quality assessment report by Flatman et al. (2016). The DHM/Point-
118 cloud product is provided in LAZ-format and in the compound coordinate system for Denmark (ETRS89 / UTM zone 32N +
119 DVR90 height - EPSG:7416). The DHM/Terrain product is a rasterized digital model of the terrain height above sea level in
120 0.4 m resolution. This product is provided in a 32-bit GeoTiff format, using the same 1 km x 1 km tiling convention and
121 spatial reference system as the DHM/Point-cloud.

122

123 **Table 1:** Overview of the data sources used for generating the EcoDes-DK15 data set. Three versions of the DHM/Pointcloud
 124 were merged to obtain a point cloud data set that contained no vegetation points scanned after 2015 and as little vegetation
 125 points before 2014 as possible. DHM/Terrain tiles were matched sources from the same data source as the corresponding point
 126 cloud tiles. A copy of the source data is archived on the internal long-term data storage at Aarhus University and is available
 127 on request. For further information see documentation on GitHub code repository and Sect. 3.6.3.

Data source	Years	Used for	Data provider	Downloaded available from (download date)	Number of tiles
DHM/Pointcloud (DHM/Punktsky)	2007-2018	Vegetation Descriptors	Danish Agency for Data Supply and Efficiency	https://kortforsyningen.dk/ (24 April 2020)	38671
DHM/Pointcloud (DHM2015_punktsky)	2007-2018	Vegetation Descriptors	Danish Agency for Data Supply and Efficiency	https://datafordeler.dk (13 September 2020)	10955
DHM/Pointcloud (GST_2014)	2007-2015	Vegetation Descriptors	Danish Agency for Data Supply and Efficiency	https://kortforsyningen.dk/ (unknown, before 2017)	47
DHM/Terrain (DHM/Terræn)	2007-2018	Terrain Descriptors	Danish Agency for Data Supply and Efficiency	https://kortforsyningen.dk/ (24 April 2020)	38671
DHM/Terrain (DHM2015_terraen)	2007-2018	Terrain Descriptors	Danish Agency for Data Supply and Efficiency	https://datafordeler.dk (13 September 2020)	10955
DHM/Terrain (GST_2014)	2007-2015	Terrain Descriptors	Danish Agency for Data Supply and Efficiency	https://kortforsyningen.dk/ (unknown, before 2017)	47

128
 129 The 1 km x 1 km tiling of the DHM/Terrain 2014/2015 and DHM/Point-cloud data sets 2014/2015 match in extent and
 130 geolocation. However, a small number of tiles ($n = 30$) in the DHM/Point-cloud data sets did not have corresponding tiles in
 131 the DHM/Terrain data sets, these were removed prior processing resulting in the total of 49673 tiles shown in Table 1.

132 2.3 Processing

133 We processed the source data using OPALS 2.3.2.0 (Pfeifer et al., 2014), Python 2.7 (Van Rossum and Drake Jr, 1995), pandas
 134 0.24.2 (Reback et al., 2019), SAGA GIS 2.3.2 (Conrad et al., 2015) from OSGeo4W64 and GDAL 2.2.4 (GDAL/OGR
 135 contributors, 2018) also from OSgeo4W64. Some re-processing was required during the peer review process, for which we
 136 used GDAL 3.3.3 from Osgeo4W64 (GDAL/OGR contributors, 2021). The large number of tiles and descriptors to be
 137 calculated, required us to develop a robust processing pipeline, which we realised as a set of Python modules. The source code
 138 is openly available via a GitHub code repository (see Sect. 6). Processing was carried out on a Dell PowerEdge R740xd

139 computational server (Windows 2012 R2 64-bit Operating System, 2x Intel Xeon Platinum 8180 Processors and 1.536TB
140 RAM). The processing of the whole data set took approximately 45 days to complete.

141

142 2.3.1 Processing workflow

143 To facilitate the processing of the large data set, we first generated a set of compact Python modules providing a programming
144 interface that allows for the calculation of the individual descriptors outlined in Sect. 3. The individual routines were then
145 integrated into a Python script mediating the processing workflow in parallel, while carrying out error handling, logging and
146 progress tracking. The schematic of the processing workflow and the Python modules is outlined in Fig. 1. Detailed information
147 is available on the GitHub repository, including instructions on how to set up the processing, documentation on the functions
148 provided by the Python modules, as well as detailed in-text commentary of the code.

149

150 We generated the processing workflow so that it should be possible to adapt it to other point cloud data sets. However, the
151 effort required in achieving this will vary depending on various features of the point cloud data set in question (such as tiling
152 and tile naming conventions, input/output grain sizes etc.). A key pre-requisite is that the point cloud is pre-classified, ideally
153 following the ASPRS LAS 1.1-1.4 standards (ASPRS, 2019). We have also provided a helper script that can be adapted to
154 generate a raster DTM from the point cloud should this not be available, see the documentation on the GitHub repository for
155 the details. Finally, the modular nature of the processing workflow allows for only a subset of the output descriptors to be
156 calculated and the integration of additional processing routines for any new user-defined descriptors.

157

Processing Workflow Overview

Inputs

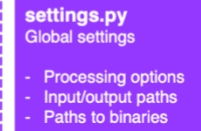
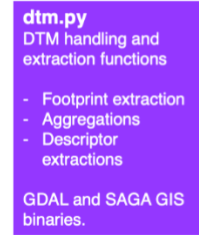
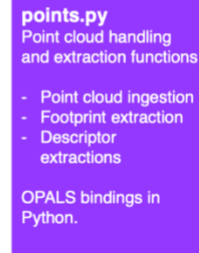
- Nationwide ALS point cloud
~ 49k tiles
- Nationwide terrain model at 0.4 m res.
~ 49k tiles



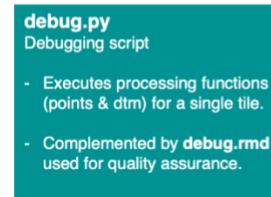
Outputs

- Ecological variables, raster 10 m res.
18 x terrain and cover structure descriptors
~ 49k tiles each

dk_lidar Python Modules



Helper scripts Independent python scripts



158

159 **Figure 1:** Diagram of the processing workflow, the *dk_lidar* Python module and helper scripts. The workflow requires two
 160 inputs: a pre-classified set of point cloud tiles and a paired set of digital terrain model (dtm) tiles. The process management is
 161 handled by the *process_tiles.py* script which facilitates processing of each tile pair (dtm and point cloud) in parallel and logs
 162 the progress. For each tile, *process_tiles.py* calls a specified set of extraction and processing functions from the *dk_lidar*
 163 modules. Point cloud extraction functions are specified in *points.py* and terrain model extraction functions are specified in
 164 *dtm.py*. The *dk_lidar* modules also contain two further files, *common.py* a script containing specifications of common functions
 165 used by the *points.py* and *dtm.py*, as well as *settings.py* which is used to set global processing options, specify file paths etc.
 166 Finally, two helper scripts are provided *progress_monitor.py* which facilitates progress monitoring and estimates the time
 167 remaining and *debug.py* a script for testing the workflow for a single tile. Together the Python scripts and modules allow to
 168 generate the ecological descriptor outputs from the two input data sets. Further documentation of the *dk_lidar* modules and
 169 workflow scripts can be found on the GitHub repository associated with this publication:
 170 <https://github.com/jakobjassmann/ecodes-dk-lidar>.

171 3 Data set description and known limitations

172 3.1 Extent, projection, resolution and data format

173 EcoDes-DK15 covers the majority of Denmark's land area, including the island of Bornholm (approximate extent: 54.56 °N
174 to 57.75 °N, 8.07 °E to 15.20 °E). The data is projected in ETRS89 UTM 32 N based on the GRS80 spheroid (EPSG: 25832).
175 The data set is available as GeoTIFFs with 10 m grain size via a data repository on Zenodo (see Sect. 6). For each descriptor
176 the nation-wide data are split into 49673 raster tiles of 1 km x 1 km with a 10 m grain size based on 25-fold aggregations of
177 the 0.4 m national grid of Denmark. A virtual raster mosaic (VRT) file is provided for each descriptor (except the
178 point_source_counts, point_source_ids and point_source_proportion descriptors), and a file containing the tile footprint
179 geometries can be used for geographical sub-setting of the data. We also provide masks for inland water and the sea.

180

181 The final data set consists of just under 94 GB of data (compressed for download 16.8 GB). To reduce the size of the data set
182 we converted numerical values from floating point precision to 16-bit integers where possible. In some cases, this required us
183 to stretch the values by a set factor to maintain information content beyond the decimal point. The descriptor conversion factors
184 are available as a csv file provided with the data set and in Table 2. Missing data (NoData) is denoted by a value of -9999
185 throughout the data set.

186 3.2 Overview and file naming convention

187 An overview of the eighteen terrain and vegetation structure descriptors as well as the auxiliary data provided can be found in
188 Table 2. Generally, the descriptor names in Table 2 reflect the prefix of the file name of a GeoTiff file within the data set. This
189 prefix is followed by a suffix representing the unique identifier for each tile based on the UTM coordinates of the tile (see
190 Sect. 3.4.3 for more detail). When working with the complete data set, tiles from the same descriptor are grouped within a
191 folder using the same descriptor name as used for the file name prefix. For example, for the tile with the unique id “6239_446”
192 the GeoTiff for the “dtm_10m” descriptor can be found in “dtm_10m/dtm_10m_6239_446.tif”. The exceptions are the point
193 counts, vegetation proportions and point source information, please see the relevant sections below for more detail.

194

195 **Table 2:** Brief overview of the eighteen main EcoDes-DK15 descriptors and descriptor groups, their ecological meaning, unit,
196 format and conversion factor. See Sect. 3.4 for a detailed description of each descriptor. In addition to the 70 raster layers for
197 the main descriptors, the data set contains nine layers of auxiliary information (see Sect. 3.7). Note: to obtain the correct unit,
198 the descriptor value needs to be divided by the conversion factor.

199

Descriptor(s)	Ecological meaning	Unit	Format	Conversion factor	Number of layers
dtm_10m	elevation	m	16-bit integer	100	1

aspect	topographic aspect	degrees	16-bit integer	10	1
slope	topographic slope	degrees	16-bit integer	10	1
heat_load_index	proxy of radiation and wetness	unitless	16-bit integer	10000	1
solar_radiation	solar radiation	MJ x 100 ⁻¹ m ⁻² x yr ⁻¹	32-bit integer	1	1
openness_mean	topographic position	degrees	16-bit integer	1	1
openness_difference	presence of linear landscape features	degrees	16-bit integer	1	1
twi	topographic wetness	unitless	16-bit integer	1000	1
amplitude_mean	complex**	undefined	32-bit float	1	1
amplitude_sd	complex**	undefined	32-bit float	1	1
canopy_height	vegetation height	m	16-bit integer	100	1
normalized_z_mean	average structural height (incl. vegetation and buildings)	m	16-bit integer	100	1
normalized_z_sd	variation in structural height (incl. vegetation and buildings)	m	16-bit integer	100	1
point_counts*	number of returns in ground, water, building and vegetation point classes; total return count and vegetation return counts in height bins	count	16-bit integer	1	30
vegetation_proportion*	proportion of vegetation returns in height bins	proportion	16-bit integer	10000	24
vegetation_density	ratio of vegetation returns to total returns	proportion	16-bit integer	10000	1
canopy_openness	ratio of ground and water returns to total returns	proportion	16-bit integer	10000	1
building_proportion	ratio of building returns to total returns		16-bit integer	10000	1
point_source_info*	point source / flight strip information	varied, see description	varied, see description	varied, see description	4
masks	inland water and sea mask	binary	16-bit integer	1	2
date_stamp*	min, max and mode of GPS dates for all vegetation points	date as YYYYMMDD***	32-bit integer	1	3

200

201 * Descriptor group containing multiple individual descriptors, see intext description for detail.

202 ** The amplitude descriptors are difficult to interpret, but can serve as useful indicators for vegetation classification and
203 biodiversity studies. Please see intext description for more detail.

204 *** YYYY = year in four digits, MM = month in two digits, DD = day in two digits.

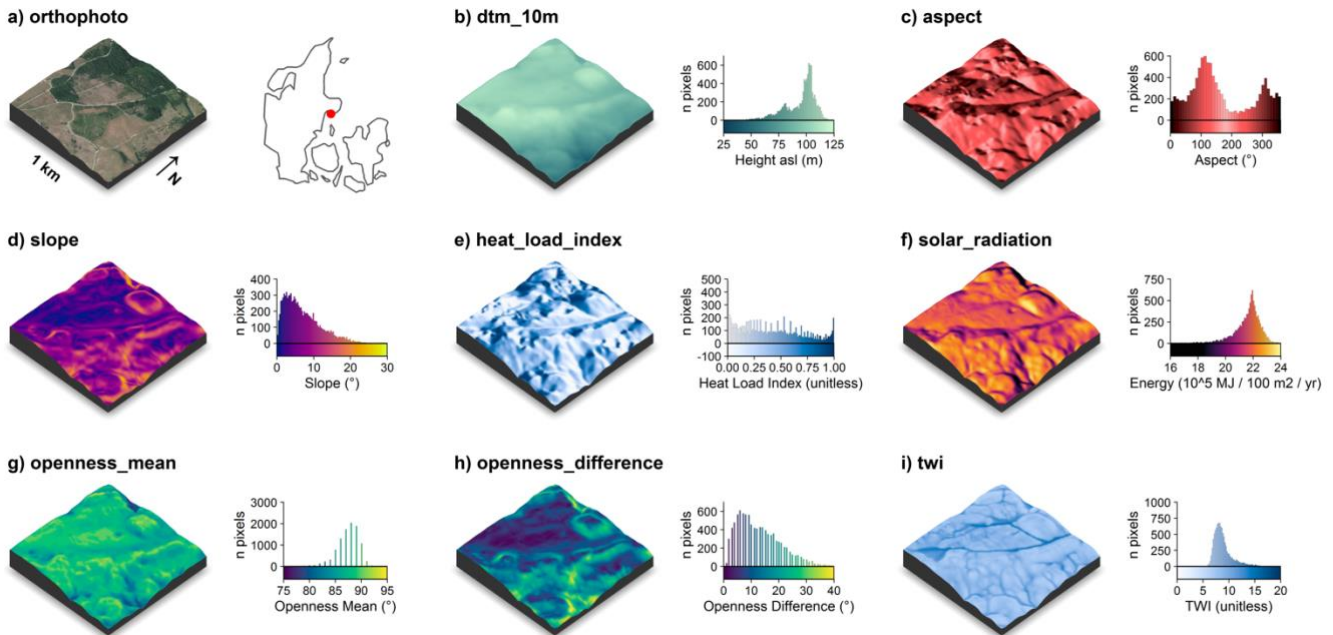
205 3.3 Completeness of the data set

206 The processing of the data set was almost completely successful. Processing failed on average for only 18 out of the 49673
207 tiles per descriptor with a maximum of 65 tiles failing for the *canoy_height*, *normalized_z_mean* and *normalized_z_sd*
208 descriptors. The majority of these tiles were located on the fringes of the data set, including sand spits, sandbanks etc, we
209 therefore did not attempt re-processing of those tiles. Instead, we generated NoData rasters for all missing descriptor - tile
210 combinations (i.e. we assigned -9999 to all cells in those tiles). We provide a text file listing the affected “NoData” tiles in the
211 folder of each descriptor (the file is named empty_tiles_XXX.txt, where XXX is the descriptor name).

212 3.4 Elevation-model derived descriptors

213 The following descriptors were solely derived from the 0.4 m digital elevation model (DHM/Terrain). Visualisations of these
214 descriptors for an example tile in the Mols Bjerger area are shown in Fig. 2.

215



216

217 **Figure 2:** Illustration of the terrain model derived descriptors for a 1 km x 1 km tile in the Mols Bjerger area (tile id: 6230_595).

218 An orthophoto and the tile location relative to Denmark are shown in (a). The terrain model (dtm_10m) is illustrated in (b).

219 The terrain derived descriptors comprise of: c) the topographic aspect, d) the topographic slope, e) the heat load index following

220 Kuehne et al. f) the estimated incident solar radiation, g) the landscape openness mean, h) the landscape openness difference
221 in the eight cardinal directions and i) the topographic wetness index (TWI) based on Kopecký et al. (2020). For visualisation
222 purposes, we amplified the altitude above sea-level by a factor of two in the 3D visualisations and divided the solar radiation
223 values by 10^5 . The 3D raster visualisations were generated using the rayshader v0.19.2 package in R (Morgan-Wall, 2020).
224 Orthophoto provided by the Danish Agency for Data Supply and Efficiency ([https://sdfc.dk/hent-data/fotos-og-geodanmark-
225 data/](https://sdfc.dk/hent-data/fotos-og-geodanmark-data/)).

226 **3.4.1 Elevation (dtm_10m)**

227 We aggregated the 0.4 m DEM by mean to match the 10 m x 10 m national grid of the remainder of the data set. We used
228 *gdalwarp* to carry out the aggregations. Values represent the elevation above sea level in metres (DVR90, EPSG: 5799)
229 multiplied by a factor of 100, rounded to the nearest integer and converted to 16-bit integer.

230 **3.4.2 Aspect (aspect)**

231 The topographic aspect describes the orientation of a slope in the terrain and may, amongst other things, be related to plant
232 growth through light and moisture availability. We calculated the aspect in degrees, with 0° indicating North, 90° East, 180°
233 South and 270° West. Values represent the aspect derived from a 10 m aggregate of the elevation model (aggregated by mean
234 with 32-bit floating point precision). Calculations were carried out using *gdaldem* binaries and the “aspect” option, which by
235 default uses Horn’s method to calculate the aspect (Horn, 1981). To avoid edge effects, all calculations were done on a mosaic
236 that included the focal tile and all available directly neighbouring tiles (maximum eight). The mosaic was cropped back to the
237 extent of the focal tile upon completion of the calculations. We then converted the value for each cell from radian to degrees,
238 multiplied it by a factor of 10, rounded to the nearest integer and stored the results as a 16-bit integer. Finally, we assigned a
239 value of -10 (-1°) to all cells where the slope was 0° (flat). Limitations in the aspect arise in relation to edge effects that occur
240 where a neighbourhood mosaic is incomplete for a focal tile (i.e., less than eight neighbouring tiles), such as for tiles along the
241 coastline or at the edge of the covered extent. For those tiles, no aspect can be derived for the rows or columns at the edge of
242 the mosaic. The cells in those rows and columns have no neighbouring cells and were assigned the NoData value (-9999).
243 Please also note that we calculated the aspect descriptor from the 10 m aggregate of the DTM/Terrain data set rather than
244 deriving it from the 0.4 m original resolution rasters and then aggregating it. The latter approach could represent the
245 aspect/slope at the original resolution better (Grohmann, 2015; Moudrý et al., 2019), but would create inconsistencies within
246 how the remaining DTM/Terrain descriptors are calculated in this dataset.

248 **3.4.3 Slope (slope)**

249 The topographic slope describes the steepness of the terrain and amongst other things may be related to moisture availability,
250 exposure and erosion. We derived the topographic slope in degrees with a 10 m grain size from a mean aggregate of the

251 elevation model (32-bit floating point precision) using the *gdaldem* binaries with the “slope” option, which by default use
252 Horn’s method to calculate the slope (Horn, 1981). To avoid edge effects, we carried out the calculations on a mosaic including
253 the focal tile and all available directly neighbouring tiles (maximum eight). The mosaic was cropped back to the extent of the
254 focal tile upon completion of the calculations. The value for each cell was converted from radian to degrees, multiplied by a
255 factor of 10, rounded to the nearest integer and stored as a 16-bit integer. Limitations in the slope arise in relation to edge
256 effects that occur where a neighbourhood mosaic is incomplete for a focal tile (i.e., less than eight neighbouring tiles), such as
257 for tiles along the coastline or at the edge of the covered extent. For those tiles, no slope can be derived for the rows or columns
258 at the edge of the mosaic. These cells in those rows and columns have no neighbouring cells and *gdaldem* assigns the NoData
259 value (-9999) to these cells. Please also note that we calculated the slope descriptor from the 10 m aggregate of the
260 DTM/Terrain data set rather than deriving it from the 0.4 m original resolution rasters and then aggregating it. The latter
261 approach could represent the aspect/slope at the original resolution better (Grohmann, 2015; Moudrý et al., 2019), but would
262 create inconsistencies within how the remaining DTM/Terrain descriptors are calculated in this dataset.

263 **3.4.4 Landscape openness mean (openness_mean)**

264 Landscape openness is a landform descriptor that indicates whether a cell is located in a depression or elevation of the
265 landscape. We calculate the landscape openness following Yokoyama et al. (2002) using the OPALS implemented algorithms.
266 We used a mean aggregate of the elevation model with 10 m grain size and 32-bit floating point precision, and derived the
267 mean landscape openness for a cell as the mean of the landscape openness in all eight cardinal directions with a search radius
268 of 150 m. We chose to base this descriptor on the aggregated 10 m elevation model and a 150 m search radius, as we think
269 that these are best suited to describe the landscape scale variation in the landforms of Denmark. Danish landscapes are
270 characterised by gently undulating terrain, valleys forged by small to medium sized rivers and dune systems along the
271 coastlines. First, we generated a mosaic including the focal tile and all available tiles in the direct neighbourhood (max. eight
272 neighbouring tiles) to reduce edge effects in subsequent calculations. The mean of the positive openness for all eight cardinal
273 directions with search radius of 150 m was then derived for all cells in the mosaic using the OPALS Openness module (options:
274 feature = 'positive', kernelSize = 15 and selMode = 0). Next, the mean openness per cell was converted from radians to degrees,
275 rounded to the nearest integer and stored as a 16-bit integer. For incomplete neighbourhood mosaics (i.e. containing less than
276 eight neighbouring tiles) we then masked out cells within the first 150 m of all edges where a neighbourhood tile was missing.
277 Finally, the output was cropped back to the extent of the focal tile. As a consequence of the edge effect related masking, the
278 focal tiles on the fringes of the data set, such as those on coastlines or at the edge of the coverage area, have no data available
279 for the first 150 m. The corresponding cells for the affected areas are set to the NoData value -9999.

280 **3.4.5 Landscape openness difference (openness_difference)**

281 In addition to the mean of the landscape openness, we also derived a landscape openness difference measure. This difference
282 measure is an indicator of whether a cell is part of a linear feature in the landscape that runs in one cardinal direction, such as

283 a ridge or valley, therefore providing additional information to the landscape openness_mean descriptor. We calculated the
284 landscape openness difference based on the 10 m mean aggregate of the elevation model (32-bit floating point precision) and
285 with a search radius of 50 m. We chose these parameters as we consider them best suited to capture the relatively narrow
286 valleys and ridgetops common in the Danish landscape. First, we generated a mosaic including the focal tile and all available
287 tiles in the direct neighbourhood (max. eight neighbouring tiles) to reduce edge effects in subsequent calculations. We then
288 calculated the minimum and maximum of the positive landscape openness from all eight cardinal directions for all cells in the
289 mosaic using the OPALS Openness module with a search radius of 50 m (feature = 'positive', kernelSize = 5 , selMode = 1
290 for minimum and selMode = 2 for maximum). Next, we converted the minimum and maximum values from radian to degrees
291 and calculated the difference between the maximum and minimum value. We rounded the result to the nearest full degree. For
292 the cases where the neighbourhood mosaic was incomplete, i.e., containing less than eight neighbouring tiles, we masked out
293 all cells within the first 50 m of all edges with a missing neighbourhood tile. The final output mosaic was then cropped to the
294 extent of the focal tile and stored as a 16-bit integer GeoTIFF. As a consequence of the edge effect related masking, focal tiles
295 on the edges of the data set, such as those on coastlines or at the edge of the coverage area, have no data available for the first
296 50 m.

297 **3.4.6 Solar Radiation (solar_radiation)**

298 Incident solar radiation is a key parameter for plant growth as it represents the electromagnetic energy available to plants
299 required for photosynthesis. However, in the comparatively flat country of Denmark, shading by other vegetation likely exerts
300 a larger influence on photosynthetic activity than terrain related shading. Here, the impact of incident solar radiation on the
301 local climate likely plays a more important role for determining plant growth due to its influence on drought/water dynamics
302 (Moeslund et al., 2019). We estimated the amount of incident solar radiation received per cell (100 m²) per year from the slope
303 and aspect computed as described above. Calculations were implemented using *gdal_calc*, following equation 3 specified in
304 McCune and Keon (2002):

305

$$306 \quad \text{solar_radiation} = 10^6 \times e^{0.339+0.808 \times \cos(L) \times \cos(S)-0.196 \times \sin(L) \times \sin(S)-0.482 \times \cos(180 - |(180 - A)|)} \times \sin(S) \quad (1)$$

307 where L is the centre latitude of the cell in degrees, S is the slope of the cell in degrees and A is the aspect of the cell in degrees.
308 The resulting estimate is given in: MJ x 100⁻¹ m⁻² x yr⁻¹ (McCune and Keon, 2002). Slope and aspect for each 10 m x 10 m
309 grid cell were sourced from the slope and aspect rasters. We saved the result as 32-bit integers. Due to propagation from the
310 calculation of slope descriptor, no solar radiation values can be calculated for cells found right on the edge of the data set, for
311 example in tiles situated along the coastline or at the edge of the sampling extent.

312 **3.4.7 Heat Load Index (heat_load_index)**

313 The heat load index (McCune and Keon, 2002) was originally developed as an indicator for temperature based solely on aspect,
314 but this characteristic is probably better captured in our solar radiation descriptor (see above) that was developed to improve
315 shortcomings in the heat load index (McCune and Keon, 2002). However, in a previous study (Moeslund et al., 2019) we show
316 that - in Denmark - the index was moderately correlated with soil moisture, and can therefore serve as a useful indicator of the
317 amount of moisture available to plants. We calculated the heat load index based on the aspect rasters (described above)
318 following the equation specified in McCune and Keon (2002) using *gdal_calc*:

319

$$heat_load_index = \frac{(1 - \cos(A - 45))}{2} \quad (2)$$

320

321 where A is the aspect in degrees. We stretched the result by a factor of 10000, rounded to the nearest integer and stored it as a
322 16-bit integer. As the `heat_load_index` is not meaningfully defined for flat cells (slope = 0° / aspect = -1°), we set the value of
323 those cells to NoData (-9999). Finally, for cells that are located on the outermost edges of the data set the `heat_load_index` is
324 not defined due to propagation of the NoData value assigned to the aspect in those cells.

325 **3.4.8 Topographic wetness index (twi)**

326 The topographic wetness index (TWI) provides a proxy measure of soil moisture or wetness based on the hydrological flow
327 modelled through a digital terrain model. Here, we derived the TWI following the method recommended by Kopecký et al.
328 (2020). We based our calculations on the aggregated 10 m elevation model (`dtm_10m`, 16-bit integer) and used a
329 neighbourhood mosaic (max. 8 neighbours) for each focal tile to derive the TWI. The exact procedure is detailed in the next
330 paragraph. As such the index values calculated by us only consider a catchment the size of one tile and all its neighbours (for
331 non-edge tiles this is a 3 km x 3 km catchment, for edge tiles it is smaller depending on the completeness of the neighbourhood
332 mosaic). We then cropped the resulting output back to the extent of the focal tile, stretched the TWI values by a factor of 1000,
333 rounded to the next full integer and stored the results as a 16-bit integer.

334 We calculated the TWI using SAGA GIS v. 7.8.2 binaries. First, we sink-filled the neighbourhood mosaic of the terrain model
335 using the `ta_preprocessor 5` module and the option “MINSLOPE 0.01” (Wang and Liu, 2006). Second, we calculated the flow
336 accumulation based on the sink-filled neighbourhood mosaic of the terrain model (from step one) using the `ta_hydrology 0`
337 module with options “METHOD 4” and “CONVERGENCE 1.0” (Freeman, 1991; Quinn et al., 1991). Third, we derived the
338 flow width and specific catchment area based on the sink-filled neighbourhood mosaic of the terrain model (from step one)
339 and the flow accumulation (from step two) using the module `ta_hydrology 19` (Gruber and Peckahm, 2008; Quinn et al., 1991).
340 Fourth, we calculated the slope based on the sink-filled neighbourhood mosaic of the terrain model (from step one) using the
341 `ta_morphometry 0` module with option “METHOD 7” (Haralick, 1983). Finally, we derived the TWI based on the specific

342 catchment area (from step three) and slope (from step four) using the module `ta_hydrology` 20 (Beven and Kirkby, 1979;
343 Böhner and Selige, 2006; Moore et al., 1991). For detailed descriptions of the modules used, please refer to the SAGA GIS
344 documentation (SAGA-GIS Tool Library Documentation v7.8.2, 2021).

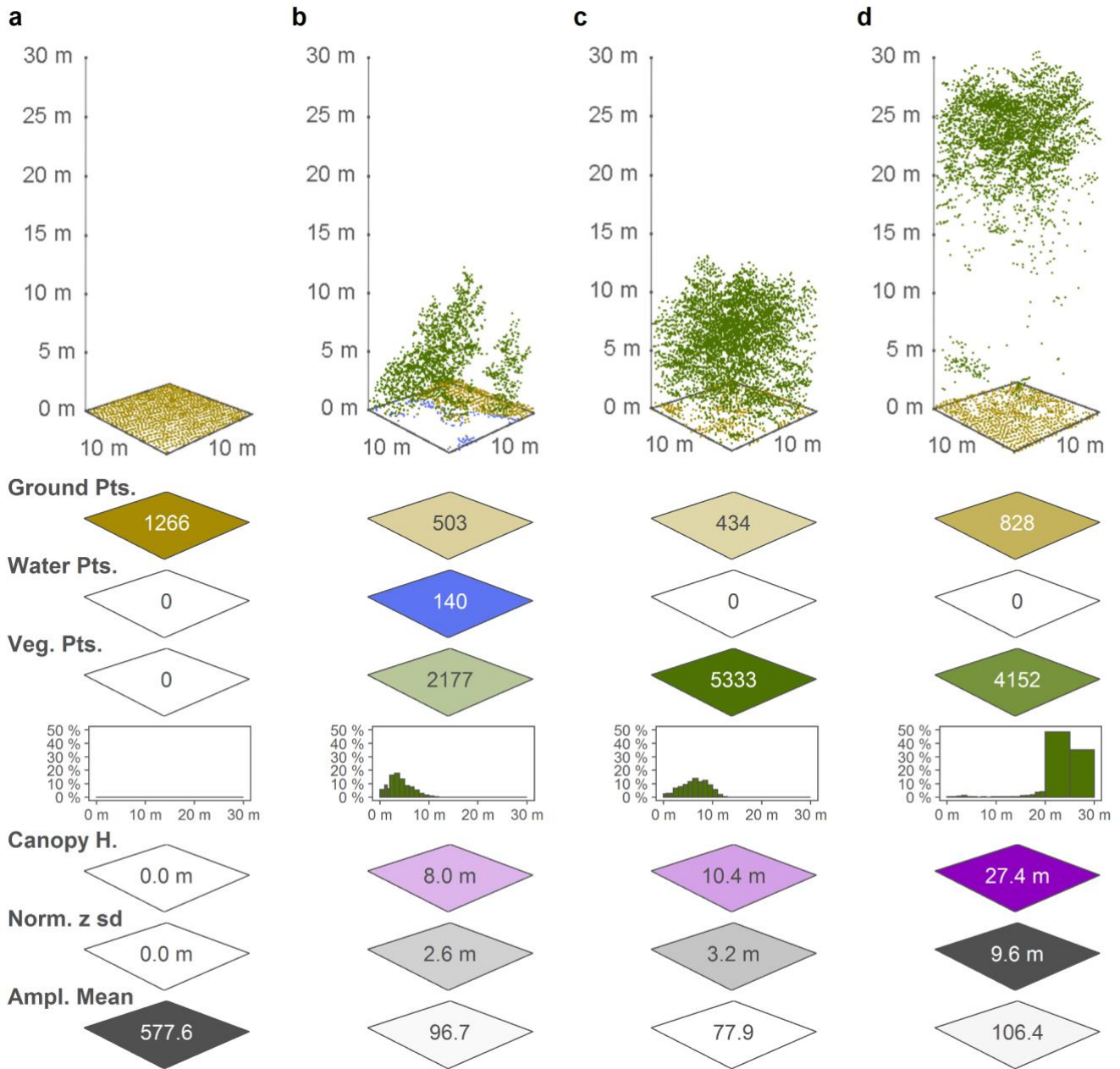
345 The TWI descriptor calculated for EcoDes-DK15 is subject to two main limitations: edge effects and small catchment size.
346 Tiles with incomplete neighbourhoods (i.e., less than 8 direct neighbours are available) will suffer from edge effects in the
347 direct vicinity of the relevant border and overall due to a reduced catchment size. Furthermore, even in the ideal case of the
348 neighbourhood being complete, for most cells flow accumulation is therefore only calculated for the direct neighbourhood of
349 a focal tile, comprising a 3 km x 3 km catchment area. While we hypothesize that, due to the relatively low variation in
350 topography in Denmark, the TWI based on this comparably small catchment area will serve as a reasonable proxy for terrain-
351 based wetness in most cases, it may be less reliable in areas with exceptionally high variation in topography or for lakes and
352 rivers with large catchments. In addition, we would like to point the reader towards the general limitations of the TWI as a
353 proxy for soil moisture or terrain wetness as for example discussed by Kopecký et al. (2020). These general limitations should
354 be taken into account when interpreting the TWI values provided in EcoDes-DK15.

355 **3.5 Point-cloud derived descriptors**

356 The DHM/Point-cloud point cloud was pre-classified into eleven point categories (Geodatastyrelsen, 2015) following the
357 ASPRS LAS 1.3 standard (ASPRS, 2011). For the EcoDes-DK15 data set, we restricted the analysis to six of these classes,
358 including ground points (“Terræn”) - class 2, water points (“Vand”) - class 9, building points (“Bygninger”) - class 6, as well
359 as low (“lav”), medium (“mellemhøj”) and high vegetation (“høj vegetation”) - classes 3, 4 and 5, respectively. We grouped
360 the three vegetation classes into one single vegetation class and, instead of the pre-assigned height categories, considered a
361 more detailed set of height bins (see point count and proportion descriptions below). The overall classification accuracy of the
362 point cloud was assessed by the Danish authorities (Flatman et al., 2016), but limited information is available for the accuracy
363 in each class. Thus, some degree of noise should be assumed across all classes. The tall vegetation category (class 6) was used
364 as a catch-all class if classification failed, as often the case for very tall buildings and structures (Flatman et al., 2016). To
365 reduce the noise related to such structures, we removed vegetation points with a normalised height exceeding 50 m above
366 ground when calculating the vegetation point counts. We included all returns, i.e., first returns and echoes, in our analysis.

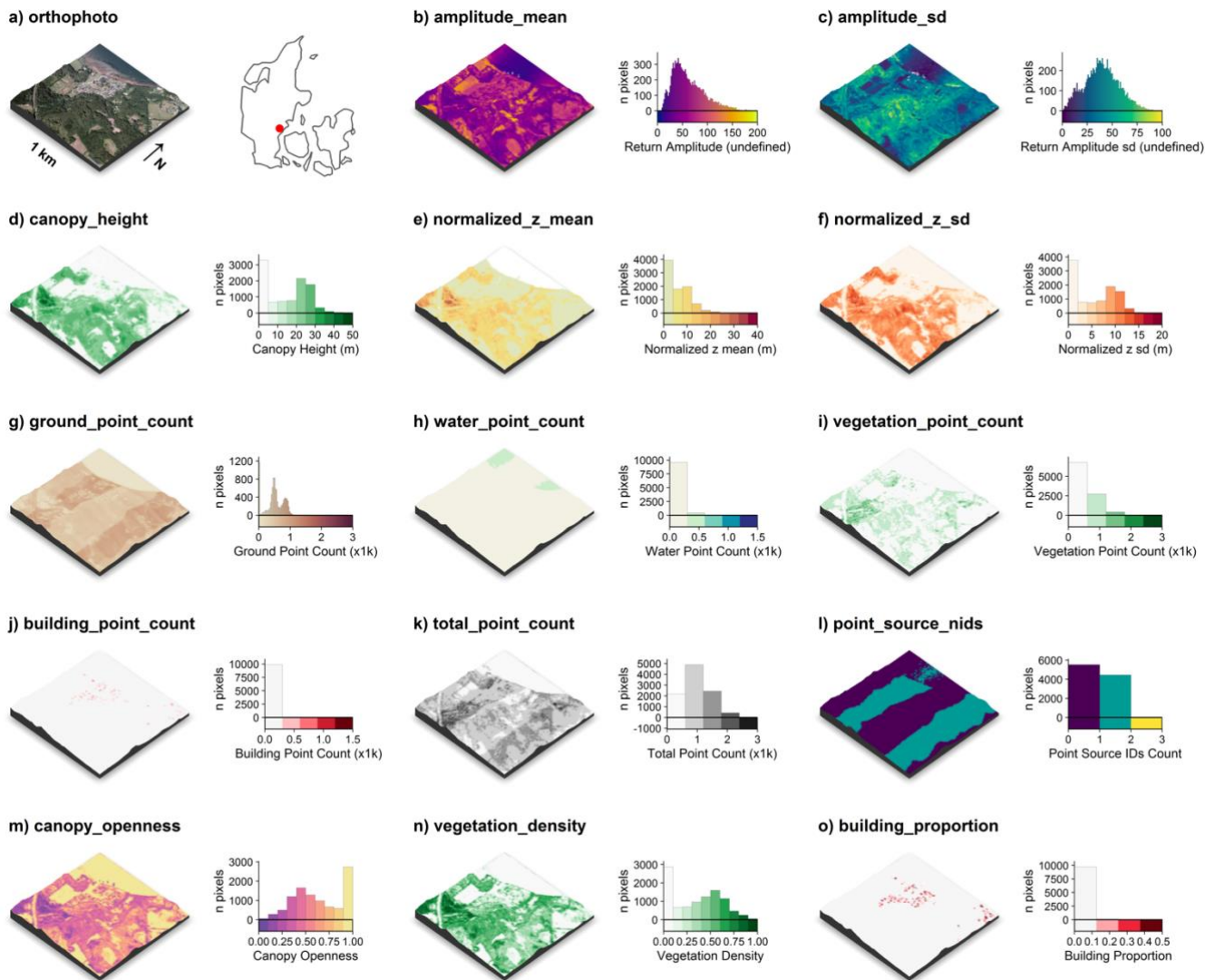
367 All point cloud processing was carried out using OPALS and the OPALS Python bindings. As none of the point cloud derived
368 descriptors required mosaicking to prevent edge-effects, we processed all point cloud descriptors on the focal tile only. After
369 the initial ingestion of the LAZ-file for a tile into the OPALS data manager format (odm), we used the *OpalsAddInfo* module
370 to add a normalised height (z) attribute to the points. For this attribute we subtracted the height of the ground derived from the
371 corresponding DHM/Terrain raster (0.4 m grid size) from the height above sea level of each point. Figure 3 illustrates how the

372 point cloud data translates to some of the descriptor outputs for four exemplary 10 m x 10 m cells from the data set, and an
 373 overview of the point cloud derived descriptors for a 1 km x 1 km tile in Vejle Fjord in central Jutland is provided in Fig. 4.



374
 375 **Figure 3:** Point cloud examples for four 10 m x 10 m cells and a selection of the associated EcoDes-DK15 descriptors derived
 376 from the point clouds, illustrating the ecological meaning and some of the limitations of the EcoDes-DK15 data set. The 10 m
 377 x 10 m cells represent the following environments: a) an agricultural field, b) the edge of a forest / parkland pond with low
 378 vegetation, c) a young plantation of dense coniferous trees, and d) old growth mixed-woodland. The EcoDes-DK15 descriptors

379 shown include (from the top) the total point counts for each cell in the three main EcoDes-DK15 categories: 1) the number of
380 returns classified as ground, 2) the number of returns classified as water and 3) the number of returns classified as vegetation.
381 In addition, the relative proportion of vegetation points per predefined height bin is illustrated below the total vegetation point
382 count. Finally, the bottom three panels show the estimated canopy height (altitude above ground for the 95%-percentile of all
383 vegetation returns), the normalized z standard deviation (variation in height above ground for all return classes), and the mean
384 return amplitude for each cell. Please note how the classification of the point cloud classification does not separate between
385 very low growing vegetation (e.g., grass) and ground points in the agricultural field shown in a), and how returns from water
386 are only registered in shallow areas close to the water bodies edge, such as exemplified by the forest pond in b). Lastly, we
387 would like to point the reader to the general limitations of ALS in penetrating forest canopies such as those shown in c) and
388 d). While the upper layers of the canopies are well resolved in both cases, the laser scanning struggles to capture some aspects
389 of the lower layers; the ground returns were frequently blocked by the thick canopy in c) and the laser fails to meaningfully
390 characterise understory vegetation and stems in d).
391



392

393 **Figure 4:** Illustration of the point cloud derived descriptors for a 1 km x 1 km tile along Vejle Fjord (tile id: 6171_541). An
 394 orthophoto and the tile location relative to Denmark are shown in (a). The point cloud derived descriptors comprise of: c) the
 395 mean return amplitude, d) the standard deviation in the return amplitude, e) the canopy height (vegetation returns only), f) the
 396 mean of the normalized height above ground (all returns), g) the mean of the normalized height (all returns), h) the ground
 397 point count, i) the water point count, j) the building point count, k) the total point count, l) the number of point sources (flight
 398 strips), m) the canopy openness, n) the vegetation density and o) the building proportion. Note the influence of point source
 399 overlap illustrated in l) on some of the descriptors, for example: g) ground point count, i) vegetation point count and k) total
 400 point count (see Sect. 3.5.5 for detail). For visualisation purposes, we amplified the altitude above sea-level by a factor of two
 401 in the 3D visualisations and divided the point counts by 1000. The 3D raster visualisations were generated using the rayshader

402 v0.19.2 package in R (Morgan-Wall, 2020). Orthophotograph provided by the Danish Agency for Data Supply and Efficiency
403 (<https://sdfe.dk/hent-data/fotos-og-geodanmark-data/>).

404 **3.5.1 Amplitude – mean and standard deviation (amplitude_mean and amplitude_sd)**

405 The amplitude attribute of a point in the DHM/Point-cloud is the actual amplitude of the return echoes, i.e., it describes the
406 strength of the LiDAR return signals detected by the sensor. The descriptor is difficult to interpret in terms of its ecological
407 meaning. Nonetheless, we believe that it is still useful for vegetation classifications, biodiversity analysis and other applications
408 that perform well with proxy data. We calculate the arithmetic mean and standard deviation of the amplitude for all points
409 within a 10 m x 10 m cell. Here, ‘all points’ refers to all points classified as ground, water, building, and vegetation points.
410 Calculations were carried using the *OPALS Cell* module and results were stored as 32-bit floats. The amplitude attributes in
411 the DHM/Point-cloud point clouds are not directly comparable when points originate from different point sources (e.g., flight
412 strips), as the amplitude has not been calibrated and hence is sensitive to differences in sensor, sensor configuration and signal
413 processing. Calculating summary metrics such as mean and standard deviation for a 10 m x 10 m cell where points from
414 different point sources are present introduces additional complexities. In some cases, a 10 m cell might contain points from up
415 to four different sources. We therefore recommend using the two amplitude descriptors with care, and - if possible - in
416 conjunction with information on the point source ids contained in the point_source_info descriptors described below.

417 **3.5.3 Canopy height (canopy_height)**

418 Canopy height is a key parameter of vegetation structure related to biomass and ecosystem functioning. We derived the canopy
419 height in metres as the 95th-percentile of the normalised height above ground of all vegetation points within each 10 m x 10
420 m cell using the *OPALS Cell* module. The resulting canopy heights were multiplied by a factor of 100, rounded to the nearest
421 integer and stored as 16-bit integers. In cases where there were no vegetation points in any given cell, we set the canopy height
422 value of the cell to zero metres. Please note that the canopy height is therefore also set as zero metres even if there are no points
423 present in the cell at all (such as ground or water points). Furthermore, our algorithm calculates the canopy height even if there
424 is only a small amount of vegetation points in a cell. In rare cases, this might lead to erroneous canopy-height readings if
425 vegetation is found on artificial structures or points have been mis-classified. For example: A tall communications tower can
426 be found just south of Aarhus and returns from the tower were miss-classified as vegetation. The resulting canopy height for
427 this cell is calculated as > 100 m above ground, which would not make sense if interpreted as a height of the vegetation above
428 ground. For such cases, the building proportion descriptor may be used to separate cells with artificial structure from those
429 with vegetation only. See also the “normalized_z” descriptor below for a closely related measure.

430 **3.5.4 Normalised height - mean and standard deviation (normalized_z_mean and normalized_z_sd)**

431 Similar to the canopy height descriptor, the normalised height describes the structure properties of the point cloud above
432 ground. The key difference between the two descriptors is that for the normalised height we also included non-vegetation

433 points (buildings & ground) and derived the summary statistic as the mean rather than the 95%-quantile. For the normalised
 434 height descriptor, we also provide a measure of variation in form of the standard deviation. Specifically, we calculated the
 435 normalised mean and the standard deviation of the mean height above ground (normalised z attribute) for all points in each 10
 436 m x 10 m grid cell using the *OPALS Cell* module. The results were multiplied by 100, rounded to the nearest integer and stored
 437 as 16-bit integers. We used the normalised z attribute generated during the ingestion of the point cloud reflecting the height of
 438 a point relative to the ground level determined by the DHM/Terrain raster. Here, all points refer to all points belonging either
 439 to the ground, water, building or vegetation class. By definition the normalised height mean will be highly correlated with the
 440 “canopy_height” descriptor for cells where mainly vegetation points are present. We kept the American spelling of the
 441 descriptor name for legacy reasons with previous versions of the data set.

442 3.5.5 Point counts (xxx_point_count_xxx)

443 The point count descriptors are intermediate descriptors used to generate the proportion descriptors described below. However,
 444 they can also be used to calculate tailored proportion descriptors relevant to addressing a specific ecological objective (see
 445 use-case example in Sect. 4.2). For EcoDes-DK15 we derived thirty point count descriptors for each 10 m x 10 m cell based
 446 on filtering of the pre-defined point classifications and separation by height above ground (normalised z) using the *OPALS*
 447 *Cell* module. All point counts were stored as 16-bit integers. These thirty descriptors contain six general point counts, including
 448 ground, water, vegetation, building and total point counts (Table 3), as well as twenty-four vegetation point counts separated
 449 in height bins (Table 4). Note that the number of returns within a 10 m cell is influenced by a) the number of point sources
 450 present in the cell, b) the relative position and distance of a cell to the point source when the data was collected (i.e., to the
 451 flight path), and c) by the point source themselves (i.e., differences between the LiDAR sensors deployed). The absolute counts
 452 are therefore not directly comparable between cells and need to be standardised first, for example by division of the total
 453 number of point counts as done for the point proportion descriptors derived by us.

454
 455 **Table 3:** General point count descriptors, as well as the height ranges and point classes included in each descriptor.
 456

Descriptor name	Height range	Point classes
ground_point_count_-01m-01m	-1 m to 1 m	ground points (class 2)
water_point_count_-01m-01m	-1 m to 1 m	water points (class 9)
ground_and_water_point_count_-01m-01m	-1 m to 1 m	ground and water points (classes 2,9)
vegetation_point_count_00m-50m	0 m to 50 m	vegetation points (classes 3,4,5)
building_point_count_-01m-50m	-1 m to 50 m	building points (class 6)
total_point_count_-01m-50m	-1 m to 50 m	ground, water, vegetation and building points (classes 2,3,4,5,6,9)

457

458 **Table 4:** Vegetation point count descriptors divided into twenty-four height bins. All vegetation point counts include the point
 459 classes 3,4 and 5.
 460

Descriptor name	Height range
vegetation_point_count_00.0m-00.5m	0.0 m to 0.5 m
vegetation_point_count_00.5m-01.0m	0.5 m to 1.0 m
vegetation_point_count_01.0m-01.5m	1.0 m to 1.5 m
vegetation_point_count_01.5m-02.0m	1.5 m to 2.0 m
vegetation_point_count_02m-03m	2 m to 3 m
vegetation_point_count_03m-04m	3 m to 4 m
vegetation_point_count_04m-05m	4 m to 5 m
vegetation_point_count_05m-06m	5 m to 6 m
vegetation_point_count_06m-07m	6 m to 7 m
vegetation_point_count_07m-08m	7 m to 8 m
vegetation_point_count_08m-09m	8 m to 9 m
vegetation_point_count_09m-10m	9 m to 10 m
vegetation_point_count_10m-11m	10 m to 11 m
vegetation_point_count_11m-12m	11 m to 12 m
vegetation_point_count_12m-13m	12 m to 13 m
vegetation_point_count_13m-14m	13 m to 14 m
vegetation_point_count_14m-15m	14 m to 14 m
vegetation_point_count_15m-16m	15 m to 16 m
vegetation_point_count_16m-17m	16 m to 17 m
vegetation_point_count_17m-18m	17 m to 18 m
vegetation_point_count_18m-19m	18 m to 19 m
vegetation_point_count_19m-20m	19 m to 20 m
vegetation_point_count_20m-25m	20 m to 25 m
vegetation_point_count_25m-50m	25 m to 50 m

461 **3.5.6 Vegetation proportions by height bin (vegetation_proportion_XXX)**

462 The vegetation proportions by height bin are amongst the key parameters in the EcoDes-DK15 data set describing vegetation
463 structure as they provide an indication of how the vegetation is distributed vertically within each cell of the raster. We
464 calculated the proportions by dividing the vegetation count for each height bin (Table 4) by the total point count
465 (total_point_count_-01m-50m) within a given 10 m x 10 m cell. Resulting proportions were multiplied by a factor of 10000,
466 rounded to the nearest integer and converted to 16-bit integers. All calculations were done using *gdal_calc* based on the
467 respective point count rasters (Sect. 3.3.5). The naming convention of the vegetation proportion descriptors
468 “vegetation_proportion_XXX” follows the same convention as the vegetation point count descriptors (Table 4), whereby the
469 suffix “XXX” is replaced with the respective height bin. Please note that height bins are spaced at 0.5 m intervals below 2 m
470 and at 1 m intervals between 2 m and 20 m. Furthermore, the range above 20 m is split into only 2 bins: 20 m to 25 m and 25
471 m to 50 m.

472 Given the properties of the DHM/Point-cloud we recommend being cautious when interpreting differences in the lower height
473 bins. It is likely that the inaccuracies in the point cloud complicate clear separation between points less than half a metre apart.
474 Furthermore, note that the proportions in the 0 m - 0.5 m bin are likely biased towards an underrepresentation of the vegetation
475 proportion in this height bin, due to challenges in separating vegetation from ground points during the pre-classification. Lastly,
476 keep in mind that dense canopy layers in the upper story of the canopy will reduce penetration of the light beam to the lower
477 canopy layers. This may result in few returns in the lower layers (for example Fig 3 d) even though perhaps vegetation is
478 present in those layers.

479 **3.5.7 Vegetation density or total vegetation proportion (vegetation_density)**

480 Vegetation density is an important component of ecosystem structure. Here, we calculated the vegetation density as the ratio
481 between the vegetation returns across all vertical height bins (vegetation_point_count_00m-50m) and the total point count
482 (total_point_count_-01m-50m). Calculations were done using *gdal_calc* based on the two point count rasters (Sect. 3.3.5).
483 Results were multiplied by 10000, rounded to the nearest integer and stored as 16-bit integers. In addition to actual difference
484 between vegetation density in a cell, the vegetation_density descriptor is also influenced by the canopy properties, e.g. a dense
485 upper layer will prevent penetration of the light beam to lower layers or even the ground, and the points sources within a cell,
486 e.g. multiple sources from different viewing angles provide a more complete estimate of the vegetation density. These
487 additional influences are important to keep in mind when interpreting the vegetation_density descriptor.

488 **3.5.7 Canopy openness, or ground and water proportion (canopy_openness)**

489 Canopy openness is an important ecological descriptor particularly of forest canopies, as it describes the amount of light
490 penetrating through to the levels of the canopy. To some degree the canopy openness serves as the inverse for the vegetation
491 density. For EcoDes-DK15, we calculated the canopy openness of a 10 m x 10 m cell as the proportion of the ground and water

492 points (ground_and_water_point_count_-01m-01m) to the total point count (total_point_count_-01m-50m) within the cell.
493 The raster calculations were done using *gdal_calc*. Results were multiplied by 10000, rounded to the nearest integer and stored
494 as 16-bit integers. Please note that the same considerations as for the vegetation_density descriptor (Sect. 3.3.7) regarding
495 canopy properties and differences in point sources between the cells apply when interpreting the canopy_openness descriptor.
496 In addition, it is important to note that building points will reduce the canopy openness the same way that vegetation points
497 would.

498 **3.5.8 Building proportion (building_proportion)**

499 In a densely populated country such as Denmark, buildings form an important part of the landscape. For ecological studies the
500 distance to buildings, their presence, absence or density may be of relevance. The building_proportion descriptor of EcoDes-
501 DK15 provides a proxy for how much building infrastructure can be found within a 10 m cell. We calculated the descriptor as
502 the number of building points (building_point_count_-01m-50m) divided by the total number of points (total_point_count_-
503 01m-50m) within each cell using *gdal_calc*. Results were multiplied by 10000, rounded to the nearest integer and stored as
504 16-bit integers. While most returns from three dimensional infrastructure are classified as buildings in the DHM/Point-cloud,
505 we would like to highlight that many roads are classified as ground (class 2) and some structures such as pylons and power
506 lines were assigned a separate class (not described in (Geodatastyrelsen, 2015)). These structures are therefore not included in
507 the building_proportion descriptor. We would further like to note that the majority of building points are likely based on returns
508 from the roofs of the buildings. Walls and other vertical structures are probably represented at a lower frequency in the point
509 clouds. Finally, we would like to point the reader to the “DCE Basemap” (Levin, 2019) which may assist in the identification
510 of basic land cover types that include buildings and other manmade structures.

511 **3.6 Auxiliary data**

512 In addition to the terrain and point cloud derived descriptors we provide three sets of auxiliary data with EcoDes-DK15. These
513 are four layers of ALS point source information, a mask for inland water and a sea mask, as well as a shapefile of the footprints
514 of the 1 km x 1 km tiles in the data set and their unique identifier.

515 **3.6.1 Point source information**

516 The point source attribute of the DHM/Point-cloud represents differences between sensor units or aircrafts that may have been
517 used during the nationwide LiDAR campaign, differences in the acquisition time and date and differences in the viewpoint or
518 acquisition angle of the cells. To aid in interpretation of descriptors that may be particularly influenced by point source, like
519 the amplitude descriptors or the vegetation proportions, we provide summary information about the point sources within each
520 10 m x 10 m cell. We summarised this information in four descriptors, the “point_source_counts”, “point_source_ids”,
521 “point_source_nids” and “point_source_proportions”. For each tile (file name suffix = tile id), these descriptors are found in
522 four subfolders bundled up in the parent “point_source_info” folder.

523 **point_source_ids** - Multi-layer raster containing one 16-bit integer layer for each point source id found in a tile. If a point
524 with a given point source id is present the value of the cell is set to the point source id (an integer number) in the respective
525 layer for the point source id, otherwise the value of a cell is set to 0. This multilayer raster can be used to match the file names
526 of the `point_source_counts` and `point_source_proportions` rasters to a given point source id. Point source ids were extracted
527 using *Opals Cell*.

528 **point_source_nids** - Single layer GeoTiff files containing the number of different point source ids in each cell stored as 16-
529 bit integers. We calculated the number of point source ids based on the `point_source_ids` descriptor using *gdal_calc*.

530 **point_source_counts** - For each tile there are multiple rasters (up to four), one raster for each point source id found in the
531 point cloud of the tile (see the *point_source_ids* descriptor). These rasters are named with an additional suffix, which matches
532 the integer point source id for which the point counts are given in the raster (e.g. `point_source_counts_xxxx_xxx_y*`, where
533 `xxxx_xxx` is the tile id and `y*` the integer point source id). The rasters contain the number of points per 10 m x 10 m cell for
534 the respective point source id in the tile. Counts were extracted using the *OPALS Cell* module and stored as 16-bit integers.

535 **point_source_proportions** - For each tile there are multiple rasters (up to four), one raster for each point source id found in
536 the point cloud of the tile (see the *point_source_ids* descriptor). These rasters are named with an additional suffix, which
537 matches the integer point source id for which the point proportions are given in the raster (e.g.
538 `point_source_proportions_xxxx_xxx_y*`, where `xxxx_xxx` is the tile id and `y*` the integer point source id). Each raster contains
539 the proportion of the point counts for a given point source id in relation to the total point count per 10 m x 10 m cell.
540 Calculations were carried out using *gdal_calc*. The final proportions were multiplied by a factor of 10000, rounded to the
541 nearest integer and stored as 16-bit integers.

542 **3.6.2 Water masks (inland_water_mask and sea_mask)**

543 We also provide rasterized water masks for use cases that require masking inland water bodies or the sea. To represent all
544 permanent lakes in Denmark, we merged three shapefiles containing (1) lakes protected by the Danish nature protection
545 legislation (§3, available at <https://arealinformation.miljoportal.dk>), (2) other valuable lakes (available on request at the
546 Danish Farming Agency in the “good farming and environmental condition” data set) and (3) a layer containing the remaining
547 rather small lakes and ponds (GeoDenmark, <https://kortforsyningen.dk/>). The combined shapefile is provided on the GitHub
548 code repository (see below). We then burned the geometries within the shapefile into the 10 m x 10 m grid using *gdal_rasterize*.
549 The masks are binary, a cell value of 1 indicates land and a value of -9999 (NoData) indicates sea or inland water, respectively.
550 When using the masks please consider that the shape, presence and absence of water bodies and coastlines may fluctuate over
551 time. We created the masks to present a snapshot of the water bodies as close as possible to the time point of the DHM/Point-
552 cloud acquisition (spring 2014 - summer 2015), but inaccuracies may still arise. When combining the data with more recent
553 observations, keep in mind that inland water bodies and coastlines may have changed since then. Finally, while we aimed to

554 produce the inland water mask to be as comprehensive as possible, some small ponds and water bodies may have been missed.
555 Note also that while some rivers are included in the sea mask, the inland water mask does not include rivers or streams. The
556 masks can be found in the “masks” subfolder of the complete data set.

557 **3.6.3 Vegetation point date stamps (date_stamp_min, date_stamp_max, date_stamp_mode)**

558 The time point at which the source data was collected may be of interest to certain applications that are using EcoDes-DK15
559 vegetation descriptors. These include for example, comparisons amongst regions where the data was collected under different
560 foliage conditions (leaf-on/leaf-off) or studies that require a precise timing of the sample such as change detection studies. To
561 better facilitate these applications, we generated three date_stamp descriptors that summarize the GPS time stamps of the
562 vegetation points within each 10 m x 10 m cell. The three descriptors are: date_stamp_min, date_stamp_max and
563 date_stamp_mode, which represent the earliest, latest and most common survey date for the vegetation points in any given cell
564 in the format “YYYYMMDD”, where YYYY is the year in four digits, MM the month in two digits and DD the day in two
565 digits.

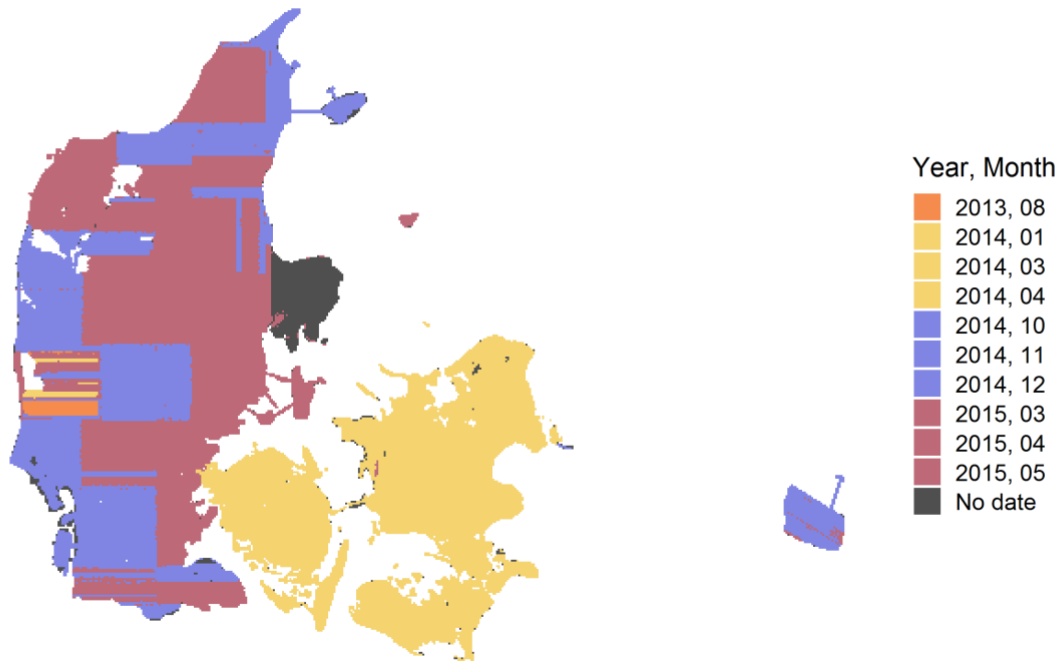
566 We used the *OPALS addInfo* module to generate a new “GPSDay” attribute for all vegetations points (classes 3,4,5) by dividing
567 the GPSTime (seconds since 6 January 1980) attribute by 86400 (seconds per day) and taking the floor value of the result. We
568 then exported the min, max and mode for each 10 m x 10 m cell using the *OPALS Cell* module, loaded the output rasters into
569 Python and converted the _GPSDay values into year, month and day in CET using the *datetime* module. Finally, we exported
570 the min, max and mode dates as 32-bit integers.

571 Note that the date_stamp descriptors only cover points that are classified as vegetation and therefore do not provide information
572 about the time point at which points belonging to other classes were surveyed (e.g., ground point, building points etc). We
573 chose to not include other point classes in the date_stamp descriptors, as we are aware that all versions of the source data sets
574 include some ground points from 2007, and as we believe that clear information about the vegetation points is most relevant
575 for the end-users conducting ecological research. Furthermore, determining the date_stamps was not possible for a proportion
576 of tiles where the GPSTime in the source data was not converted from seconds per GPS week to GPS time in seconds since 6
577 January 1980. A post-hoc conversion is not possible without the knowledge of the exact GPS week number, which is not
578 provided in the source data. In these cases, we assigned the NoData value to the date_stamps. The majority of the tiles affected
579 is located in the areas around Mols Bjerge and Sønderborg (Fig. 5). However, from auxiliary information about the source data
580 sets we know that these areas were surveyed April-May 2015 and October 2014, respectively.

581

EcoDes-DK15 Vegetation Point Collection Dates

Aggregate of date_stamp_mode for each tile



582

583

584

585

586

587

588

589

Figure 5: Distribution of the most common survey date for the vegetation points in each tile of the EcoDes-DK15 dataset. The data shown is aggregated for each tile from date_stamp_mode descriptor. The figure highlights that while the majority of the vegetation points is from 2014/15, the data set also includes a small amount of vegetation points from 2013 in western Jutland. Furthermore, surveys were conducted in all seasons, with vegetation points originating in spring, summer, autumn and winter. Nonetheless, the majority of vegetation points comes from the leaf-off season. Lastly, the date_stamp descriptors could not be derived for some regions as the GPSTime was not provided in the point clouds. However, from auxiliary information we know that the surveys in the Mols Bjerger and Sønderborg areas were conducted in April-May 2015 and October 2014, respectively.

590

3.6.4 Footprint file (tile_footprints.shp)

591

592

593

To assist data access and creation of data subsets, we have produced an ESRI shapefile containing the footprints of all 1 km x 1 km tiles in the EcoDes-DK15 data set. The shapefile was generated based on the “dtm_10m” rasters and the tile identifier of each footprint geometry is specified in the “tile_id” attribute column.

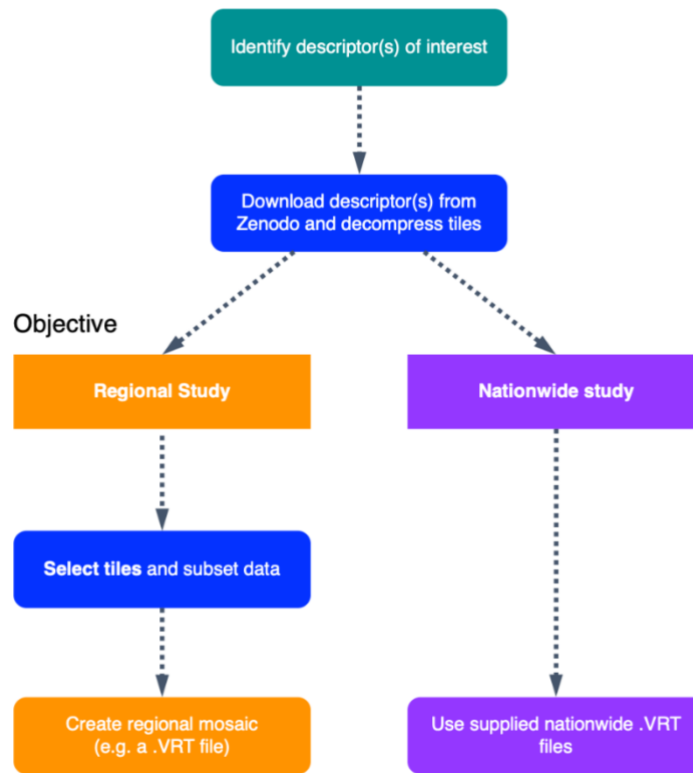
594 **4. Data access and ecological use case example**

595 **4.1 Data access and handling**

596 Depending on the extent of the study, it may be preferable to work with a subset of the data set rather than the nationwide VRT
597 files (Fig. 6). We suggest starting by identifying the relevant EcoDes-DK15 descriptors of interest, then retrieving the relevant
598 data from the repository and decompressing the archives (instructions provided on data repository). If the study area of interest
599 covers a large fraction of Denmark's extent and sufficient processing power is available, the nationwide VRT data should
600 provide the most convenient access to the selected descriptors. However, if the study area does not cover a large proportion of
601 Denmark, then we suggest sub setting the data using the tile footprints to decrease demands on computational resources. After
602 sub setting, local / regional VRT files or mosaics can be generated if needed. We provide an example R script illustrating how
603 this sub setting could be done for the use case example shown in the next section on the code repository
604 ([manuscript/figure 7/subset_data set.R](#)). We have also made the resulting subset available as a “teaser” (5 MB) to help the
605 reader assess the value of EcoDes-DK15 without having to commit to the multi-gigabyte download of the complete data set
606 (see Sect. 6).

607

Data access

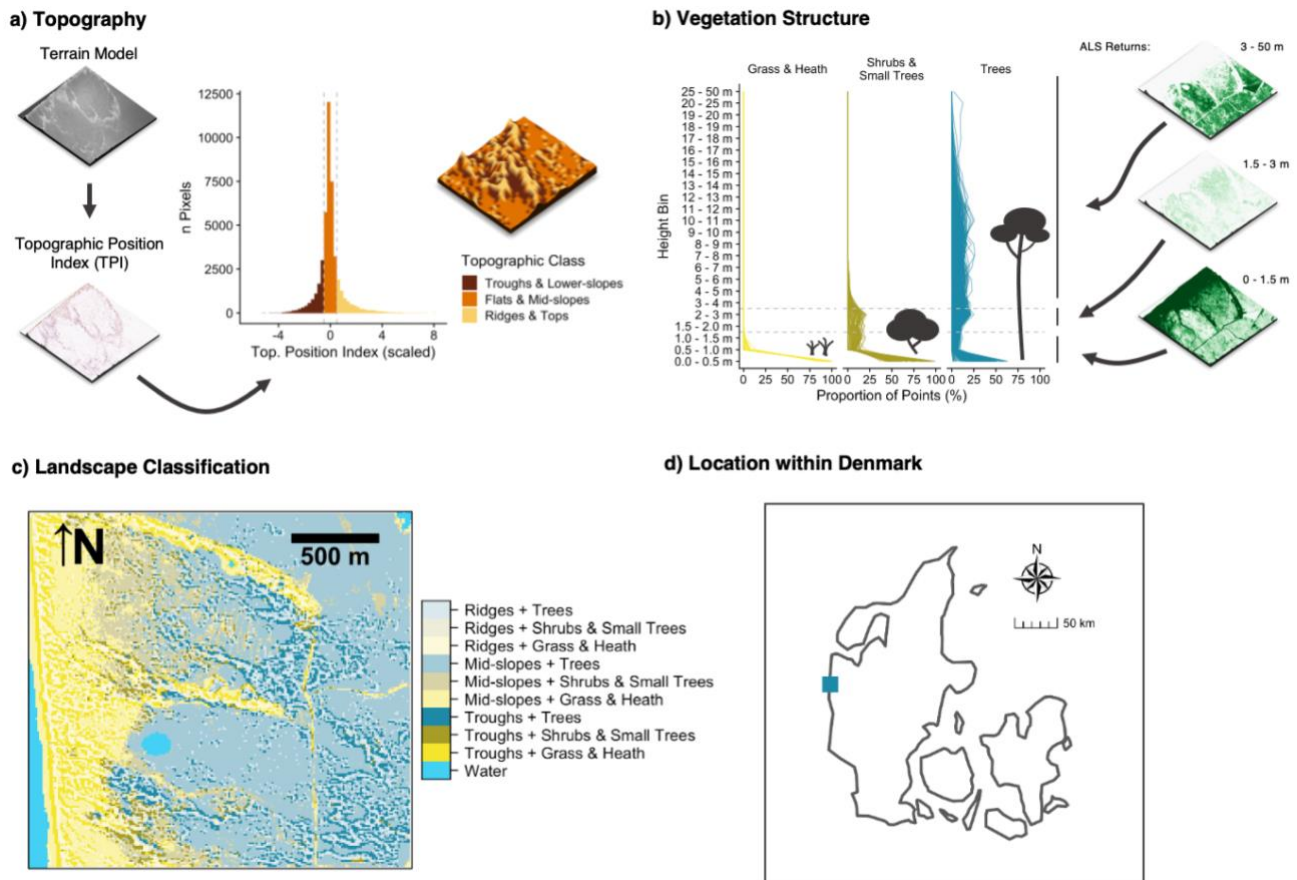


608

609 **Figure 6:** Schematic chart of two possible approaches for accessing and integrating EcoDes-DK15 data into ecological studies.
610 The first step is to identify which descriptors are of interest, these descriptors can then be downloaded from the Zenodo
611 repository and decompressed. Next a decision needs to be made whether the whole data set (nationwide) or only a subset of
612 the tiles is required (e.g., a regional study). As the whole data set is relatively large (~94 GB), storage and processing limitations
613 need to be taken into account when planning data processing and handling. If a subset of tiles is sufficient for a study, the
614 provided tile footprints can be used to identify which tiles are required based on a geometry (e.g., a shapefile) of the study
615 region(s). Finally, for easy data handling in subsequent analysis, a mosaic of the selected tiles can be created. For nationwide
616 use we provided virtual mosaics (VRT files) containing all tiles for the descriptors. An R script illustrating how the sub setting
617 can be done for a regional study can be found on the GitHub repository: [https://github.com/jakobjassmann/ecodes-dk-](https://github.com/jakobjassmann/ecodes-dk-lidar/blob/master/manuscript/figure_7/subset_dataset.R)
618 [lidar/blob/master/manuscript/figure_7/subset_dataset.R](https://github.com/jakobjassmann/ecodes-dk-lidar/blob/master/manuscript/figure_7/subset_dataset.R).

619 **4.2 Use case example - ecological landscape stratification of Husby Klit nature protected area**

620 Figure 7 illustrates a use case for the EcoDes-DK15 data set with an example of an ecologically motivated landscape
621 stratification of the “Husby Klit” old-dune protected area in western Denmark. We developed this stratification for a group of
622 Master’s projects carrying out vegetation monitoring in the area. Our aim was to capture the variation in the dominant
623 vegetation based on vegetation structure as well as the variation in fine-scale topography created by the dune systems across
624 the landscape. In addition to using the descriptors already provided, the stratification required us to derive a topographic
625 position index as well as grouping the point densities in height bins relevant to the characteristics of the three most common
626 dominant vegetation types (grass and heath, *Pinus mugo* Turra, *Pinus sylvestris* L.) in the area. The source code for this figure
627 contained in the code repository provides an example of how this can be achieved ([manuscript/figure 7/figure 7.R](#)).
628



629

630 **Figure 7:** Use-case example: Landscape stratification of the Husby Klit protected area based on EcoDes-DK15 derived terrain
631 and vegetation structure descriptors. The target was to stratify the landscape of the Husby Klit “dune plantation” area in the
632 west of Denmark (56.2837 - 56.3024 °N, 8.1239 - 8.1600 °E) to facilitate stratified random sampling for vegetation monitoring.

633 We identified the four tiles overlapping with the boundaries of the protected area and derived a stratification based on two
634 components: topographic position (a) and vegetation structure (b). We hypothesized that both components would influence
635 the vegetation communities present. For the topographic position (a), we first derived and standardised the topographic position
636 index (TPI) (Weiss, 2001) from the terrain model (dtm_10m). Following (Weiss, 2001) we then classified each cell based on
637 the scaled TPI into three categories. A scaled TPI below a value of -0.5 was classified as a “trough or lower-slope”, a scaled
638 TPI between -0.5 and 0.5 as “mid-slope or flat”, and a scaled TPI above 0.5 as a “ridge or top”. For the vegetation structure
639 component (b), we calculated the proportion of returns in three simplified height bins: 1) 0 m to 1.5 m, 2) 1.5 m to 3.0 m and
640 3) 3.0 m - 50 m. Here we included both ground and vegetation returns as the divisor for the standardisation, but not the returns
641 from buildings or water. Based on *a priori* knowledge we deduced that there are three dominant vegetation communities within
642 the protected area: communities dominated by grass and heath with vegetation growth generally below 1.5 m, communities
643 dominated by shrubs and small trees (including the invasive *Pinus mugo*) with vegetation growth predominantly below 3.0 m,
644 and communities dominated by trees (including the native *Pinus sylvestris*), generally with growth above 3.0 m. We used this
645 knowledge to assign the three vegetation classes based on the proportion of point returns in the simplified height bins. For the
646 “grass and heath” class we used a strict cut off with no points present above 1.5 m. For the “shrubs and small trees” class we
647 used a fuzzy cut off allowing the proportion of points in the 3.0 m and above bin to reach up to 10% of the maximum proportion
648 found in this height bin. All remaining cells were then assigned to the “trees” class. Finally, we combined the two classifications
649 into one as illustrated in c). Panel d) shows the location of the protected area within Denmark. The 3D raster visualisations
650 were generated using the rayshader v0.19.2 package in R (Morgan-Wall, 2020).

651 **5. Discussion - limitations and future perspectives**

652 Our data set demonstrates how the complex information in ALS point cloud data sets spanning more than 40.000 km², can be
653 condensed into a compact data set of rasterized descriptors of interest for ecological studies. For the whole of Denmark, we
654 provide 70 raster layers representing eighteen measures that describe a snapshot of vegetation height, structure and density, as
655 well as topography and topography-derived habitat characteristics, including slope, aspect, solar radiation and wetness for the
656 time period 2014-2015. These measures are of direct relevance for ecological research on species’ habitat characteristics,
657 distribution modelling, biodiversity and conservation applications. Condensing the ALS derived information into a compact
658 set of raster descriptors makes it more accessible to the community of ecological researchers and practitioners, allowing them
659 to access information on the vertical structure of vegetation and terrain otherwise difficult to obtain for large extents such as
660 those of a whole country.

661 We would like to highlight some key ecological and physical limitations that should be kept in mind when using the data or
662 derivatives. Firstly, we were able to only carry out a simple qualitative assessment of the errors in the EcoDes-DK14 data set
663 within the scope of this project. All descriptors should therefore be seen as proxies for the geographical and biological

664 properties they describe. Errors in the original point cloud and DTM will have propagated through to the final descriptors and
665 future studies are needed to assess to which degree the proxy measures correlate with in-field data. Furthermore, the EcoDes
666 data set is a snapshot in time representing the state of the vegetation in the one and a half years between spring 2014 and
667 summer 2015 (with some exception in western Jutland, where the data is from 2013). Like anywhere on Earth, the landscapes
668 of Denmark may change over time and by the time point of publication of this data set over 5 years may have passed since the
669 collection of the source data. External data sources containing information about on-going or past changes (such as satellite
670 imagery - see below) might help overcome this bias. Additionally, the geographical differences in the timing of the point cloud
671 collection across the country (see Sect 6.3.4) may introduce noise and could affect cross-comparability of the data between
672 regions, for example due to seasonal differences in foliage (see e.g., Leiterer et al., 2015). Furthermore, there are implicit
673 limitations in spatial scale due to the set grain size of the data set. We chose a 10 m x 10 m grid for efficiency in computation
674 and data handling, as well as to overcome limitations in the density of the source point cloud (four to five points per m²). Our
675 data set might therefore not serve well for capturing some ecological relevant variation in terrain and vegetation structures at
676 scales below the 10 m x 10 m grain size. We believe that our data set is nonetheless valuable in providing ecologically relevant
677 information at the geographical extent of Denmark.

678 While some of the descriptors in the presented data set such as elevation, slope and vegetation height are quite straightforward
679 to interpret, the ecological meaning of other descriptors – for example those related to vegetation structure – may not be as
680 obvious as they are influenced by multiple ecological and sensing methodology related factors. The *amplitude*, *point count*
681 and *point proportion* descriptors are amongst those measures. For example, while the (non-calibrated) amplitude in the
682 DHM/Point-cloud source data may generally relate to the reflectance properties of the surface that generated the return, the
683 incident light angle, scattering and subsequent generation of echoes may result in several different surfaces generating similar
684 amplitude signatures. Furthermore, the point counts may be influenced by a whole suite of factors, including incident light
685 angle, scattering, density of flight strips covering a given cell, as well as canopy properties - most importantly the penetration
686 ability. While standardising the point counts as proportions to the total counts may help to account for some of these factors,
687 it is likely that notable uncertainties will remain even in the proportions especially for lower layers of the canopy. Nonetheless,
688 we believe that these measures can be informative if appropriate care is taken in their interpretation.

689 Two code developments could enhance the EcoDes-DK15 processing workflow in efficiency and transferability: using gdal
690 Python bindings and switching to an open-source point cloud handler. First, for practical reasons we reverted to using gdal
691 binaries rather than the Python bindings as we encountered issues with the gdal bindings provided by the OPALS shell on our
692 computational server. Solving this issue and using the bindings instead of the binaries could reduce hard drive access time and
693 overheads from launching subprocesses and therefore potentially speed up the raster manipulations in the workflow. However,
694 as the point cloud processing takes the majority of time (we estimate 75-80%) we did not invest further resources to do so in
695 the first development round. Secondly, while our Python source code is open source and freely available, OPALS itself requires

696 the purchase of a software license, limiting the transferability of our code to projects which can afford the license. We did not
697 explore alternatives to OPALS, but a redeveloped processing pipeline could make use of purely open source software
698 benefiting from ongoing developments in the field, see for example the “Laserchicken” Python module (Meijer et al., 2020)
699 and “lidR” R package (Roussel et al., 2020).

700

701 We believe that to realise the full potential of ALS derived data such as EcoDes-DK15 these data sets are ideally combined
702 with other data sources including climate, field data and remote sensing observations. Climate data is especially relevant for
703 addressing research on species-habitat relationships, distribution models and biodiversity studies and many studies have
704 demonstrated the power of ALS observations in complementing climate data for such exercises (Coops et al., 2016; Zellweger
705 et al., 2016). Like for other remote sensing products, field data is essential for validating inferences and putting biological
706 meaning into ALS data (Coops et al., 2021) - this applies especially to the more complex structural vegetation measures in
707 EcoDes-DK15. This could be achieved through field surveys combined with terrestrial and drone based ALS data, where the
708 point density is much higher (e.g., Madsen et al., 2020). The potential benefits from fusing ALS data with other remote sensing
709 products have been realised early on (Hyde et al., 2005) and demonstrated again since then (e.g., Coops et al., 2021;
710 Montgomery et al., 2019; Manzanera et al., 2016). However, note that data fusion does not provide additional value in every
711 use case (Xu et al., 2018; Ceballos et al., 2015; Boelman et al., 2016). We still believe that there is tremendous potential in
712 combining EcoDes-DK15 with other types of remote sensing data. Fine-grain optical imagery could provide proxies for
713 horizontal vegetation structure in grasslands where the vegetation is too small to be captured by the DHM/Point-cloud density
714 (e.g., Malmstrom et al., 2017; Pazúr et al., 2021) and satellite derived time-series can provide unique temporal perspectives
715 that describe parameters of seasonality (e.g., Boelman et al., 2016) and the historical context on disturbances and landcover
716 change not captured in the single time-point ALS data (e.g., Senf et al., 2017; Pekel et al., 2016).

717 **6. Data availability**

718 The data is openly available under a Creative Commons by Attribution 4.0 license on Zenodo:

719 <https://doi.org/10.5281/zenodo.4756556> (Assmann et al., 2021)

720

721 A small example subset “teaser” (5 MB) covering the 9 km x 9 km of the Husby Klit area (Fig. 7) is available on the GitHub
722 code repository:

723 https://github.com/jakobjassmann/ecodes-dk-lidar/blob/master/manuscript/figure_7/EcoDes-DK15_teaser.zip

724

725 **7. Code availability**

726 The source code for the processing pipeline is openly available under a simplified BSD license via GitHub:

727 <https://github.com/jakobjassmann/ecodes-dk-lidar>

728 **8. Conclusions**

729 Open data sets like EcoDes-DK15 will allow ecologists with limited computational resources and little expertise in handling
730 LiDAR point clouds to use large-scale ALS data for their research. We see our efforts not only as a first step for providing
731 ready-to-use descriptors of local vegetation and terrain features, but also for providing an example workflow and tools that
732 allow for the replication of the processing. We have described and documented the measures of terrain and vegetation structure
733 contained in the data set and pointed out possible applications and limitations. We are confident that EcoDes-DK15 provides
734 a meaningful collection of ecological descriptors at a 10 x 10 m resolution for the extent of a whole country and we encourage
735 the community to use our workflow and collection of codes as inspiration to process other large-scale ALS data sets in a similar
736 manner. Ultimately, we hope the publication of this data set will help facilitate the uptake of ALS-derived information by
737 ecological researchers and practitioners in Denmark and beyond.

738 **9. Author contributions**

739 All co-authors developed the data set with focus on its ecological relevance, providing input on the ecological meaning, spatial
740 scale and calculation of the descriptors. JJA developed the code with input from JEM. JJA carried out the computations. JJA
741 led the writing of the manuscript, with all co-authors contributing to the manuscript in a collaborative manner. SN provided
742 funding and supervision for this project.

743 **10. Competing interests**

744 The authors declare that they have no conflict of interest.

745 **11. Acknowledgements**

746 We would like to thank Andràs Zlinszky for his contributions to earlier versions of the data set, Charles Davison for feedback
747 regarding data use and handling, as well as Matthew Barbee and Zsófia Koma for sharing their insights on the source data
748 merger and Zsófia's script to generate summary statistics for the different versions of the DHM point clouds. Funding for this
749 work was provided by the Carlsberg Foundation (Distinguished Associate Professor Fellowships) and Aarhus University

750 Research Foundation (AUFF-E-2015-FLS-8-73) to Signe Normand (SN). This work is a contribution to SustainScapes –
751 Center for Sustainable Landscapes under Global Change (grant NNF200C0059595 to SN).

752 **12. References**

753 Ackermann, F.: Airborne laser scanning—present status and future expectations, *ISPRS J PHOTOGRAMM*, 54, 64–67,
754 [https://doi.org/10.1016/S0924-2716\(99\)00009-X](https://doi.org/10.1016/S0924-2716(99)00009-X), 1999.

755 ASPRS: LAS Specification Version 1.3 - R11, American Society for Photogrammetry & Remote Sensing, Bethesda, Maryland,
756 2011.

757 ASPRS: LAS Specification 1.4 - R14, American Society for Photogrammetry and Remote Sensing, Bethesda, Maryland, 2019.

758 Assmann, J. J., Moeslund, J. E., Treier, U. A., and Normand, S.: EcoDes-DK15: High-resolution ecological descriptors of
759 vegetation and terrain derived from Denmark’s national airborne laser scanning data set, Zenodo [data set],
760 <https://doi.org/10.5281/zenodo.4756556>, 2021.

761 Bakx, T. R. M., Koma, Z., Seijmonsbergen, A. C., and Kissling, W. D.: Use and categorization of Light Detection and Ranging
762 vegetation metrics in avian diversity and species distribution research, *Divers Distrib*, 25, 1045–1059,
763 <https://doi.org/10.1111/ddi.12915>, 2019.

764 Beven, K. J. and Kirkby, M. J.: A physically based, variable contributing area model of basin hydrology / Un modèle à base
765 physique de zone d’appel variable de l’hydrologie du bassin versant, *Hyrdol Sci B*, 24, 43–69,
766 <https://doi.org/10.1080/02626667909491834>, 1979.

767 Boelman, N. T., Holbrook, J. D., Greaves, H. E., Krause, J. S., Chmura, H. E., Magney, T. S., Perez, J. H., Eitel, J. U. H.,
768 Gough, L., Vierling, K. T., Wingfield, J. C., and Vierling, L. A.: Airborne laser scanning and spectral remote sensing give a
769 bird’s eye perspective on arctic tundra breeding habitat at multiple spatial scales, *Remote Sens Environ*, 184, 337–349,
770 <https://doi.org/10.1016/j.rse.2016.07.012>, 2016.

771 Böhner, J. and Selige, T.: Spatial Prediction Of Soil Attributes Using Terrain Analysis And Climate Regionalisation, *Göttinger*
772 *Geographische Abhandlungen*, 115, 13–120, 2006.

773 Ceballos, A., Hernández, J., Corvalán, P., and Galleguillos, M.: Comparison of Airborne LiDAR and Satellite Hyperspectral
774 Remote Sensing to Estimate Vascular Plant Richness in Deciduous Mediterranean Forests of Central Chile, *Remote Sens-*
775 *Basel*, 7, 2692–2714, <https://doi.org/10.3390/rs70302692>, 2015.

776 Conrad, O., Bechtel, B., Bock, M., Dietrich, H., Fischer, E., Gerlitz, L., Wehberg, J., Wichmann, V., and Böhner, J.: System
777 for Automated Geoscientific Analyses (SAGA) v. 2.1.4, *Geosci Model Dev*, 8, 1991–2007, [https://doi.org/10.5194/gmd-8-](https://doi.org/10.5194/gmd-8-1991-2015)
778 [1991-2015](https://doi.org/10.5194/gmd-8-1991-2015), 2015.

779 Coops, N. C., Tompaski, P., Nijland, W., Rickbeil, G. J. M., Nielsen, S. E., Bater, C. W., and Stadt, J. J.: A forest structure
780 habitat index based on airborne laser scanning data, *Ecol Indic*, 67, 346–357, <https://doi.org/10.1016/j.ecolind.2016.02.057>,
781 2016.

782 Coops, N. C., Tompalski, P., Goodbody, T. R. H., Queinnec, M., Luther, J. E., Bolton, D. K., White, J. C., Wulder, M. A., van
783 Lier, O. R., and Hermosilla, T.: Modelling lidar-derived estimates of forest attributes over space and time: A review of
784 approaches and future trends, *Remote Sens Environ*, 260, 112477, <https://doi.org/10.1016/j.rse.2021.112477>, 2021.

785 Flatman, A., Rosenkranz, B., Evers, K., Bartels, P., Kokkendorff, S., Knudsen, T., and Nielsen, T.: Quality assessment report
786 to the Danish Elevation Model (DK-DEM), Agency for Data Supply and Efficiency, Copenhagen, Denmark, 2016.

787 Freeman, T. G.: Calculating catchment area with divergent flow based on a regular grid, *Comput Geosci*, 17, 413–422,
788 [https://doi.org/10.1016/0098-3004\(91\)90048-I](https://doi.org/10.1016/0098-3004(91)90048-I), 1991.

789 Froidevaux, J. S. P., Zellweger, F., Bollmann, K., Jones, G., and Obrist, M. K.: From field surveys to LiDAR: Shining a light
790 on how bats respond to forest structure, *Remote Sens Environ*, 175, 242–250, <https://doi.org/10.1016/j.rse.2015.12.038>, 2016.

791 GDAL/OGR contributors: GDAL/OGR Geospatial Data Abstraction software Library, Open Source Geospatial Foundation,
792 2018.

793 GDAL/OGR contributors: GDAL/OGR Geospatial Data Abstraction software Library, Open Source Geospatial Foundation,
794 2021.

795 Geodatastyrelsen: Dataspecifikation for Danmarks Højdemodel Punktsky. Data version 2.0 - Januar 2015., Geodatastyrelsen,
796 Copenhagen, 2015.

797 Grohmann, C. H.: Effects of spatial resolution on slope and aspect derivation for regional-scale analysis, *Computers &
798 Geosciences*, 77, 111–117, <https://doi.org/10.1016/j.cageo.2015.02.003>, 2015.

799 Gruber, S. and Peckahm, S.: Land-Surface Parameters and Objects in Hydrology, in: *Geomorphometry: Concepts, Software,
800 Applications*, vol. 33, edited by: Hengl, T. and Reuter, H. I., Elsevier, 293–308, 2008.

801 Guo, X., Coops, N. C., Tompalski, P., Nielsen, S. E., Bater, C. W., and John Stadt, J.: Regional mapping of vegetation structure
802 for biodiversity monitoring using airborne lidar data, *Ecol Inform*, 38, 50–61, <https://doi.org/10.1016/j.ecoinf.2017.01.005>,
803 2017.

804 Haralick, R. M.: Ridges and valleys on digital images, *Comput Vision Graph*, 22, 28–38, [https://doi.org/10.1016/0734-
189X\(83\)90094-4](https://doi.org/10.1016/0734-
805 189X(83)90094-4), 1983.

806 Horn, B. K. P.: Hill shading and the reflectance map, *P IEEE*, 69, 14–47, <https://doi.org/10.1109/PROC.1981.11918>, 1981.

807 Hyde, P., Dubayah, R., Peterson, B., Blair, J. B., Hofton, M., Hunsaker, C., Knox, R., and Walker, W.: Mapping forest structure
808 for wildlife habitat analysis using waveform lidar: Validation of montane ecosystems, *Remote Sens Environ*, 96, 427–437,
809 <https://doi.org/10.1016/j.rse.2005.03.005>, 2005.

810 IPBES: Global assessment report on biodiversity and ecosystem services of the Intergovernmental Science-Policy Platform on
811 Biodiversity and Ecosystem Services., edited by: Brondizio, E. S., Díaz, S., and Settele, J., IPBES secretariat, Bonn, Germany.,
812 2019.

813 Kopecký, M., Macek, M., and Wild, J.: Topographic Wetness Index calculation guidelines based on measured soil moisture
814 and plant species composition, *Sci Total Environ*, 143785, <https://doi.org/10.1016/j.scitotenv.2020.143785>, 2020.

815 Leiterer, R., Furrer, R., Schaepman, M. E., and Morsdorf, F.: Forest canopy-structure characterization: A data-driven approach,
816 *Forest Ecology and Management*, 358, 48–61, <https://doi.org/10.1016/j.foreco.2015.09.003>, 2015.

817 Leutner, B. F., Reineking, B., Müller, J., Bachmann, M., Beierkuhnlein, C., Dech, S., and Wegmann, M.: Modelling Forest α -
818 Diversity and Floristic Composition — On the Added Value of LiDAR plus Hyperspectral Remote Sensing, *Remote Sens*-
819 *Basel*, 4, 2818–2845, <https://doi.org/10.3390/rs4092818>, 2012.

820 Levin, G.: Basemap03. Technical documentation of the method for elaboration of a land-use and land-cover map for Denmark,
821 Aarhus University, DCE – Danish Centre for Environment and Energy, Aarhus, Denmark, 2019.

822 Lin, Y., Vosselman, G., Cao, Y., and Yang, M. Y.: Active and incremental learning for semantic ALS point cloud
823 segmentation, *ISPRS J PHOTOGRAMM*, 169, 73–92, <https://doi.org/10.1016/j.isprsjprs.2020.09.003>, 2020.

824 Lopatin, J., Dolos, K., Hernández, H. J., Galleguillos, M., and Fassnacht, F. E.: Comparing Generalized Linear Models and
825 random forest to model vascular plant species richness using LiDAR data in a natural forest in central Chile, *Remote Sens*
826 *Environ*, 173, 200–210, <https://doi.org/10.1016/j.rse.2015.11.029>, 2016.

827 Madsen, B., Treier, U. A., Zlinszky, A., Lucieer, A., and Normand, S.: Detecting shrub encroachment in seminatural grasslands
828 using UAS LiDAR, *Ecol Evol*, 10, 4876–4902, <https://doi.org/10.1002/ece3.6240>, 2020.

829 Malmstrom, C. M., Butterfield, H. S., Planck, L., Long, C. W., and Eviner, V. T.: Novel fine-scale aerial mapping approach
830 quantifies grassland weed cover dynamics and response to management, *PLOS ONE*, 12, e0181665,
831 <https://doi.org/10.1371/journal.pone.0181665>, 2017.

832 Manzanera, J. A., García-Abril, A., Pascual, C., Tejera, R., Martín-Fernández, S., Tokola, T., and Valbuena, R.: Fusion of
833 airborne LiDAR and multispectral sensors reveals synergic capabilities in forest structure characterization, *GISci Remote Sens*,
834 53, 723–738, <https://doi.org/10.1080/15481603.2016.1231605>, 2016.

835 Mao, L., Dennett, J., Bater, C. W., Tompalski, P., Coops, N. C., Farr, D., Kohler, M., White, B., Stadt, J. J., and Nielsen, S.
836 E.: Using airborne laser scanning to predict plant species richness and assess conservation threats in the oil sands region of
837 Alberta’s boreal forest, *Forest Ecol Manag*, 409, 29–37, <https://doi.org/10.1016/j.foreco.2017.11.017>, 2018.

838 McCune, B. and Keon, D.: Equations for potential annual direct incident radiation and heat load, *J Veg Sci*, 13, 603–606,
839 <https://doi.org/10.1111/j.1654-1103.2002.tb02087.x>, 2002.

840 Meijer, C., Grootes, M. W., Koma, Z., Dzigan, Y., Gonçalves, R., Andela, B., van den Oord, G., Ranguelova, E., Renaud, N.,
841 and Kissling, W. D.: Laserchicken—A tool for distributed feature calculation from massive LiDAR point cloud datasets,
842 *SoftwareX*, 12, 100626, <https://doi.org/10.1016/j.softx.2020.100626>, 2020.

843 Moeslund, J. E., Arge, L., Bøcher, P. K., Dalgaard, T., Odgaard, M. V., Nygaard, B., and Svenning, J.-C.: Topographically
844 controlled soil moisture is the primary driver of local vegetation patterns across a lowland region, *Ecosphere*, 4, art91,
845 <https://doi.org/10.1890/ES13-00134.1>, 2013.

846 Moeslund, J. E., Zlinszky, A., Ejrnæs, R., Brunbjerg, A. K., Bøcher, P. K., Svenning, J.-C., and Normand, S.: Light detection
847 and ranging explains diversity of plants, fungi, lichens, and bryophytes across multiple habitats and large geographic extent,
848 *Ecol Appl*, 29, e01907, <https://doi.org/10.1002/eap.1907>, 2019.

849 Montgomery, J., Brisco, B., Chasmer, L., Devito, K., Cobbaert, D., and Hopkinson, C.: SAR and Lidar Temporal Data Fusion
850 Approaches to Boreal Wetland Ecosystem Monitoring, *Remote Sens-Basel*, 11, 161, <https://doi.org/10.3390/rs11020161>,
851 2019.

852 Moore, I. D., Grayson, R. B., and Ladson, A. R.: Digital terrain modelling: A review of hydrological, geomorphological, and
853 biological applications, *Hydrol Process*, 5, 3–30, <https://doi.org/10.1002/hyp.3360050103>, 1991.

854 Morgan-Wall, T.: rayshader: Create Maps and Visualize Data in 2D and 3D, 2020.

855 Moudrý, V., Lecours, V., Malavasi, M., Misiuk, B., Gábor, L., Gdulová, K., Šímová, P., and Wild, J.: Potential pitfalls in
856 rescaling digital terrain model-derived attributes for ecological studies, *Ecological Informatics*, 54, 100987,
857 <https://doi.org/10.1016/j.ecoinf.2019.100987>, 2019.

858 Moudrý, V., Klápště, P., Fogl, M., Gdulová, K., Barták, V., and Urban, R.: Assessment of LiDAR ground filtering algorithms
859 for determining ground surface of non-natural terrain overgrown with forest and steppe vegetation, *MEASUREMENT*, 150,
860 107047, <https://doi.org/10.1016/j.measurement.2019.107047>, 2020.

861 Nord-Larsen, T., Riis-Nielsen, T., and Ottosen, M. B.: Forest resource map of Denmark: Mapping of Danish forest resource
862 using ALS from 2014-2015, Department of Geosciences and Natural Resource Management, University of Copenhagen,
863 Copenhagen, Denmark, 2017.

864 Pazúr, R., Huber, N., Weber, D., Ginzler, C., and Price, B.: A national extent map of cropland and grassland for Switzerland
865 based on Sentinel-2 data, *Earth Syst Sci Data*, 1–14, <https://doi.org/10.5194/essd-2021-60>, 2021.

866 Pekel, J.-F., Cottam, A., Gorelick, N., and Belward, A. S.: High-resolution mapping of global surface water and its long-term
867 changes, 540, 418–422, <https://doi.org/10.1038/nature20584>, 2016.

868 Peura, M., Silveyra Gonzalez, R., Müller, J., Heurich, M., Vierling, L. A., Mönkkönen, M., and Bässler, C.: Mapping a ‘cryptic
869 kingdom’: Performance of lidar derived environmental variables in modelling the occurrence of forest fungi, *Remote Sens*
870 *Environ*, 186, 428–438, <https://doi.org/10.1016/j.rse.2016.09.003>, 2016.

871 Pfeifer, N., Mandlbürger, G., Otepka, J., and Karel, W.: OPALS – A framework for Airborne Laser Scanning data analysis,
872 *Comput Environ Urban*, 45, 125–136, <https://doi.org/10.1016/j.compenvurbsys.2013.11.002>, 2014.

873 Quinn, P., Beven, K., Chevallier, P., and Planchon, O.: The prediction of hillslope flow paths for distributed hydrological
874 modelling using digital terrain models, *Hydrol Process*, 5, 59–79, <https://doi.org/10.1002/hyp.3360050106>, 1991.

875 Reback, J., McKinney, W., Bossche, J. V. den, jbrockmendel, Augspurger, T., Cloud, P., gfyong, Sinhrks, Klein, A., Tratner,
876 J., She, C., Roeschke, M., Petersen, T., Ayd, W., Hayden, A., Hawkins, S., Schendel, J., Garcia, M., Jancauskas, V., Battiston,
877 P., Seabold, S., chris-b1, h-vetinari, Hoyer, S., Overmeire, W., Mehayar, M., nouri, behzad, Kluyver, T., Whelan, C., and Chen,
878 K. W.: pandas-dev/pandas: v0.24.2, Zenodo, <https://doi.org/10.5281/zenodo.3509135>, 2019.

879 Roussel, J.-R., Auty, D., Coops, N. C., Tompalski, P., Goodbody, T. R. H., Meador, A. S., Bourdon, J.-F., de Boissieu, F., and
880 Achim, A.: lidR: An R package for analysis of Airborne Laser Scanning (ALS) data, *Remote Sens Environ*, 251, 112061,
881 <https://doi.org/10.1016/j.rse.2020.112061>, 2020.

882 SAGA-GIS Tool Library Documentation v7.8.2: http://www.saga-gis.org/saga_tool_doc/7.8.2/index.html, last access: 28 June
883 2021.

884 Senf, C., Pflugmacher, D., Hostert, P., and Seidl, R.: Using Landsat time series for characterizing forest disturbance dynamics
885 in the coupled human and natural systems of Central Europe, *ISPRS J Photogramm*, 130, 453–463,
886 <https://doi.org/10.1016/j.isprsjprs.2017.07.004>, 2017.

887 Sithole, G. and Vosselman, G.: Experimental comparison of filter algorithms for bare-Earth extraction from airborne laser
888 scanning point clouds, *ISPRS J PHOTOGRAMM*, 59, 85–101, <https://doi.org/10.1016/j.isprsjprs.2004.05.004>, 2004.

889 Thers, H., Brunbjerg, A. K., Læssøe, T., Ejrnæs, R., Bøcher, P. K., and Svenning, J.-C.: Lidar-derived variables as a proxy for
890 fungal species richness and composition in temperate Northern Europe, *Remote Sens Environ*, 200, 102–113,
891 <https://doi.org/10.1016/j.rse.2017.08.011>, 2017.

892 Tweedy, P. J., Moriarty, K. M., Bailey, J. D., and Epps, C. W.: Using fine scale resolution vegetation data from LiDAR and
893 ground-based sampling to predict Pacific marten resting habitat at multiple spatial scales, *Forest Ecol Manag*, 452, 117556,
894 <https://doi.org/10.1016/j.foreco.2019.117556>, 2019.

895 Valbuena, R., O'Connor, B., Zellweger, F., Simonson, W., Vihervaara, P., Maltamo, M., Silva, C. A., Almeida, D. R. A.,
896 Danks, F., Morsdorf, F., Chirici, G., Lucas, R., Coomes, D. A., and Coops, N. C.: Standardizing Ecosystem Morphological
897 Traits from 3D Information Sources, *Trends Ecol Evol*, S0169534720300811, <https://doi.org/10.1016/j.tree.2020.03.006>,
898 2020.

899 Van Rossum, G. and Drake Jr, F. L.: Python reference manual, Centrum voor Wiskunde en Informatica Amsterdam, 1995.

900 Vierling, K. T., Vierling, L. A., Gould, W. A., Martinuzzi, S., and Clawges, R. M.: Lidar: shedding new light on habitat
901 characterization and modeling, *Front Ecol Environ*, 6, 90–98, <https://doi.org/10.1890/070001>, 2008.

902 Vo, A.-V., Laefer, D. F., and Bertolotto, M.: Airborne laser scanning data storage and indexing: state-of-the-art review, *Int J*
903 *Remote Sens*, 37, 6187–6204, <https://doi.org/10.1080/01431161.2016.1256511>, 2016.

904 Wagner, W., Ullrich, A., Ducic, V., Melzer, T., and Studnicka, N.: Gaussian decomposition and calibration of a novel small-
905 footprint full-waveform digitising airborne laser scanner, *ISPRS J Photogramm*, 60, 100–112,
906 <https://doi.org/10.1016/j.isprsjprs.2005.12.001>, 2006.

907 Wang, L. and Liu, H.: An efficient method for identifying and filling surface depressions in digital elevation models for
908 hydrologic analysis and modelling, *Int J Geogr Inf Sci*, 20, 193–213, <https://doi.org/10.1080/13658810500433453>, 2006.

909 Weiss, A.: Topographic position and landforms analysis, in: Poster presentation, ESRI user conference, San Diego, CA, 2001.

910 Xu, C., Manley, B., and Morgenroth, J.: Evaluation of modelling approaches in predicting forest volume and stand age for
911 small-scale plantation forests in New Zealand with RapidEye and LiDAR, *Int J Appl Earth Obs*, 73, 386–396,
912 <https://doi.org/10.1016/j.jag.2018.06.021>, 2018.

913 Yokoyama, R.: Visualizing Topography by Openness: A New Application of Image Processing to Digital Elevation Models,
914 *Photogramm Eng Rem S*, 68, 257–265, 2002.

915 Zellweger, F., Baltensweiler, A., Ginzler, C., Roth, T., Braunisch, V., Bugmann, H., and Bollmann, K.: Environmental
916 predictors of species richness in forest landscapes: abiotic factors versus vegetation structure, *J Biogeogr*, 43, 1080–1090,
917 <https://doi.org/10.1111/jbi.12696>, 2016.
918